Journal of South American Earth Sciences 174 (2026) 105983

Contents lists available at ScienceDirect

Journal of South American Earth Sciences

journal homepage: www.elsevier.com/locate/jsames

A window into a middle Eocene mesotrophic mixed siliciclastic-carbonate system from the South American Pacific margin (Paracas Formation, Pisco Basin, Peru)

Giovanni Coletti [a], Luca Mariani [b,a,*], Elisa Malinverno [a], Alberto Vimercati [a], Claudio Di Celma [c], Alberto Collareta [d], Giancarlo Molli [d], Giovanni Sarti [d], Giovanni Bianucci [d], Orangel Aguilera [e], Alessandro Cavallo [a], Mario Urbina [f], Giulia Bosio [a,d]

[a] Dipartimento di Scienze dell'Ambiente e della Terra, Università degli Studi di Milano-Bicocca, Milano, Italy
[b] Dipartimento di Scienze Chimiche e Geologiche, Università degli Studi di Modena e Reggio Emilia, Modena, Italy
[c] Scuola di Scienze e Tecnologie, Università di Camerino, Camerino, Italy
[d] Dipartimento di Scienze della Terra, Università di Pisa, Pisa, Italy
[e] Fluminense Federal University (UFF), Paleoecology and Global Changes Laboratory, Campus Gragoatá, Bloco M, No. 110, CEP: 24210-200, Niterói, Rio de Janeiro, Brazil
[f] Museo de Historia Natural - Universidad Nacional Mayor de San Marcos, Lima, Peru

ARTICLE INFO

Keywords:
Lepidocyclinids
Paleogene
Los Choros member
Shallow-water carbonates
Hothouse

ABSTRACT

The Paracas Formation of the Pisco Basin (southern Peru) includes the lower Los Choros Member and the upper Yumaque Member and preserves key paleoenvironmental information on the shallow-marine tropical ecosystems of the eastern Pacific in middle Eocene times. This study focuses on five stratigraphic sections and a few minor outcrops of the Los Choros Member exposed in the Ica Desert. Sedimentological observations, X-ray diffraction data, and micropaleontology reveal a vertical transition from coarse-grained, mixed siliciclastic-carbonate bioclastic deposits resting unconformably on the pre-Cenozoic basement, to finer-grained fossiliferous mudstones of the overlying Yumaque Member. Large benthic foraminifera from the Los Choros Member and nannofossils from the base of the overlying Yumaque Member constrain the deposition of the former to around 43 Ma. Skeletal assemblages include both large and small benthic foraminifera along with mollusks, barnacles, red algae, echinoderms and bryozoans, pointing to a warm-temperate to tropical, shallow-marine setting characterized by moderate hydrodynamic energy and mesotrophic conditions. Despite being taxonomically distinct, the carbonate-producing systems of the paleo-Pacific display functional similarities with the coeval Tethys platforms. These systems evolved independently until the Oligocene, when lepidocyclinids expanded into the Tethys, thereby replacing rapidly the indigenous, nummulitid-dominated faunas. The factors behind the evolutionary success and dispersal of the lepidocyclinids are still largely unknown, but the sedimentological and paleoecological features of the Los Choros strata suggest that thermal adaptability played a major role.

1. Introduction

Our understanding of the Earth's paleoenvironmental and paleobiological history during the Cenozoic is strongly based on the record of the (Neo)Tethys Ocean, the sea that used to separate the northern continental blocks of Laurasia and Cimmeria from the southern continental block of Gondwana (Stampfli, 2000). This ocean began to develop towards the end of the Paleozoic (Stampfli, 2000; Muttoni et al., 2009) and has survived ever since, albeit in a diminished form, its latest remnants being the modern eastern Mediterranean Sea. For obvious historical reasons, geological research has focused heavily on this region, often overlooking the coeval processes occurring along the margins of the much wider Panthalassa. The latter, most of which evolved into the modern Pacific Ocean, was characterized by its own faunal and floral assemblages, especially following the opening of the Atlantic Ocean during the Early Cretaceous. This divergence is clearly reflected in the Eocene shallow-marine paleontological record.

Following the latest Paleocene, elevated global temperatures

* Corresponding author. Dipartimento di Scienze Chimiche e Geologiche, Università degli Studi di Modena e Reggio Emilia, Modena, Italy
E-mail address: l.mariani35@unimore.it (L. Mariani).

https://doi.org/10.1016/j.jsames.2026.105983
Received 26 November 2025; Received in revised form 19 January 2026; Accepted 29 January 2026
Available online 31 January 2026

reshaped tropical assemblages, triggering a decline in the abundance of symbiont-bearing, reef-building, colonial corals (reef corals) and a concomitant rise in both the diversity and abundance of symbiont-bearing large benthic foraminifera (hereinafter, LBF) (Pomar et al., 2017; Aguilera et al., 2020; Coletti et al., 2022; Benedetti et al., 2024; Ali et al., 2025; Bosellini et al., 2025). Throughout most of the Eocene, these unicellular organisms were the main shallow-marine benthic carbonate producers (Coletti et al., 2022). However, while Tethyan LBF assemblages were largely represented by nummulitids (e.g., *Nummulites*, *Assilina*, *Operculina*), lepidocyclinids (e.g., *Helicostegina*, *Helicolepidina*, *Polylepidina*, *Lepidocyclina*) were the most diagnostic and abundant taxa along the coasts of the proto-Pacific (BouDagher-Fadel, 2018). The latter group diverged from an *Amphistegina*-like ancestor during the middle Eocene (Adams, 1987; Butterlin, 1984, 1990; BouDagher-Fadel and Price, 2010; Mitchell et al., 2022), migrated to West Africa during the early Oligocene, and then rapidly colonized the whole Tethys (BouDagher-Fadel and Price, 2010).

The Pisco Basin is a Cenozoic forearc basin that developed along the Pacific margin of South America from the Eocene to the Pliocene (e.g., Dunbar et al., 1990; Di Celma et al., 2022). It is widely recognized for its outstanding fossil record of marine vertebrates (Bianucci and Collareta, 2022), including some of the largest organisms that ever inhabited the Earth's oceans (Lambert et al., 2010; Collareta et al., 2017; Bianucci et al., 2023), and for the exquisite preservation of its fossil assemblages (Bianucci et al., 2018; Bosio et al., 2021, 2025a).

Beyond its significance in documenting marine vertebrate evolution, the Pisco Basin provides crucial evidence for understanding the dynamics of the Eocene hothouse carbonate factories along the proto-Pacific coasts, offering insights into the overarching characteristics of these LBF-dominated systems. Accordingly, the primary objective of this study is to provide a comprehensive, detailed, and quantitative analysis of the shallow-marine skeletal assemblages of the Los Choros Member of the Eocene Paracas Formation of the Pisco Basin. These data are compared with those from coeval middle Eocene shallow-water deposits from the Eurasian Tethys to identify fundamental differences and similarities. Such a comparison highlights the primary processes and underlying drivers governing the development of the LBF-dominated carbonate-producing environments. These types of systems are not nearly as common today as they use to be during the Paleogene hothouse earth (Coletti et al., 2022; Bialik et al., 2023). However, due to the current rapid warming trend of Earth's surface, they may happen to spread once again as coral-dominated carbonate factories collapse.

2. Geological setting

The Peruvian coast is studded with a series of Cenozoic forearc basins, including the Pisco Basin (Thornburg and Kulm, 1981; Kulm et al., 1982). The onshore portion of this basin, referred to as the East Pisco Basin, is bounded by the Western Cordillera to the northeast and the Coastal Cordillera to the southwest, and was exhumed during the

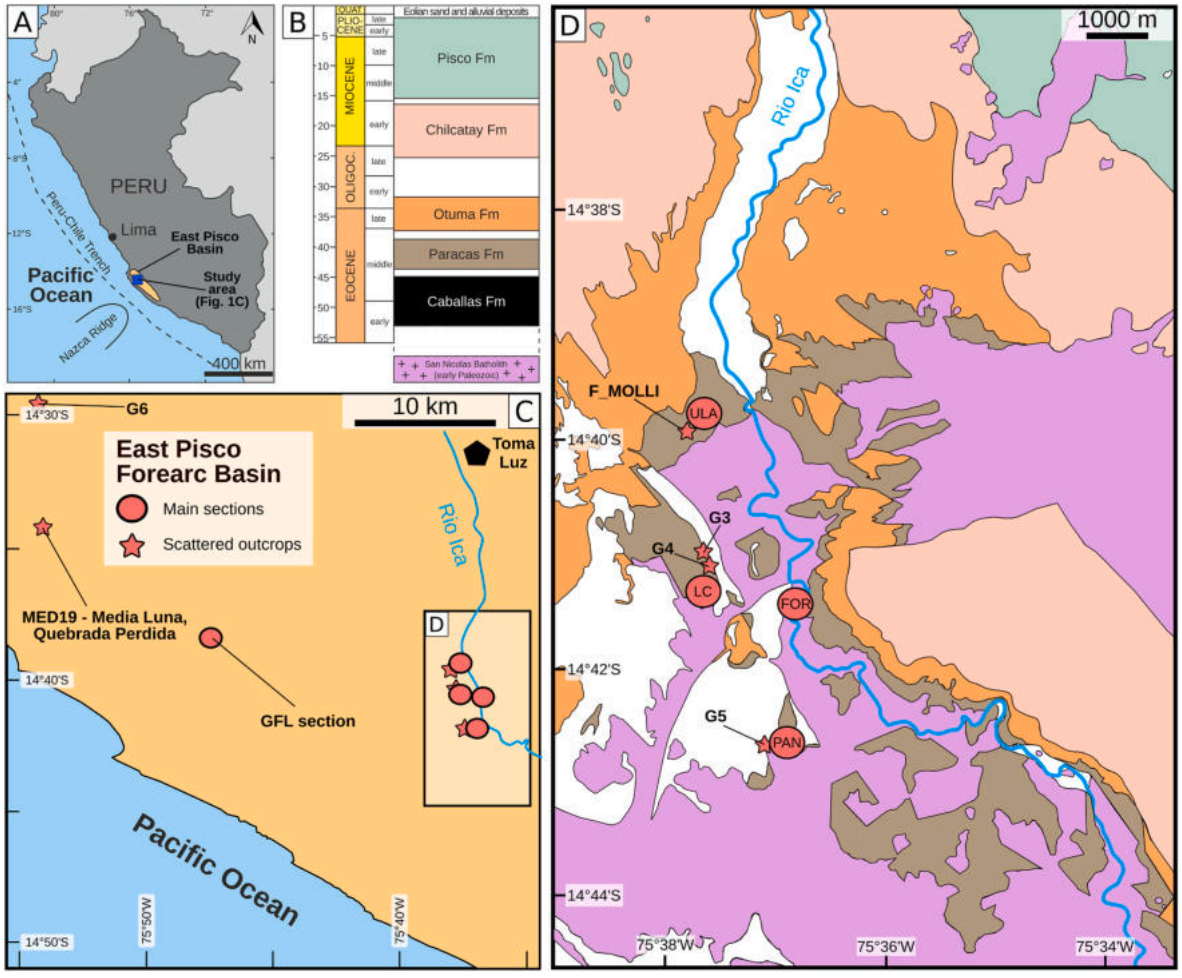

Fig. 1. Geographic and geological maps of the study area. A) Location of the East Pisco Basin and the study area in Southwestern Peru. B) Overall stratigraphy of the East Pisco Basin. C) Detail of the study area showing the investigated sites within the Ica Desert Valley, reporting the geographic location of the main sections and outcrops, in the vicinities of Toma Luz. D) Geological map of the area shown in the inset panel D reported in Figure C where most of the investigated sections and scattered outcrops are located.

Quaternary as a result of the subduction of the submarine Nazca Ridge under the largely continental South American plate (Hsu, 1992; Macharé and Ortlieb, 1992; Hampel, 2002; Romero et al., 2013; Ciattoni et al., 2025) (Fig. 1).

Between the Eocene and the Pliocene, prior to its eventual exhumation, the Pisco Basin experienced significant subsidence (Viveen and Schlunegger, 2018), facilitating the deposition of a thick sedimentary succession onto a complex crystalline basement. This basement consists of Proterozoic rocks of the Arequipa Massif (Ramos, 2008) intruded by Paleozoic granitoids of the San Nicolás Batholith (Mukasa and Henry, 1990). The basin-filling sedimentary succession includes: the lower Eocene Caballas Formation, the middle Eocene Paracas Formation, the upper Eocene to lower Oligocene Otuma Formation, the Lower Miocene Tunga and Chilcatay Formations, the Middle to Upper Miocene Pisco Formation, and the Quaternary Cañete Formation (Dunbar et al., 1990; León et al., 2008a,b; DeVries, 1998, 2017; DeVries et al., 2017, 2024; DeVries and Jud, 2018; Di Celma et al., 2022; Malinverno et al., 2025) (Fig. 1).

Our study area is located along the western side of the lower Ica River Valley in the Ica Desert. Here, Eocene deposits are represented by the Paracas and Otuma formations (DeVries, 2017, 2019), which together comprise Di Celma et al.'s (2022) Megasequence P (Fig. 1). The Paracas Formation records a transgressive, deepening upward cycle, which consists of basal siliciclastic sandstones of the Los Choros Member passing upward into diatomaceous siltstones of the overlying Yumaque Member (DeVries et al., 2017; Malinverno et al., 2021). The Los Choros Member comprises shallow-water, coarse-grained, mixed siliciclastic-calcareous bioclastic deposits. Its skeletal assemblage is dominated by LBF, with common acorn barnacles, mollusks, echinoids, and shark teeth, alongside rarer bryozoans and coralline algae (Morales et al., 2010, 2013; Coletti et al., 2019). The dominance of LBF suggests a tropical to warm-temperate paleoenvironment, and their taxonomic composition indicates a Lutetian age between 43.6 Ma and 42.37 Ma (Coletti et al., 2019). The directly overlying Yumaque Member consists of mixed siliciclastic-bioclastic siltstones rich in marine microfossils, yielding biostratigraphic ages between 42.37 Ma and ca. 37.88/37.46 Ma, corresponding to a time interval ranging from the late Lutetian to the Bartonian-Priabonian transition (Dunbar et al., 1990; DeVries, 1998; DeVries et al., 2006; Lambert et al., 2017, 2019; Malinverno et al., 2021).

3. Material and methods

3.1. Sample collection and fieldwork

The stratigraphy of the Paracas Formation was investigated through detailed fieldwork conducted in the Ica Desert (southern Peru), focusing on the Los Choros Member and the lowermost intervals of the Yumaque Member. Four reference stratigraphic sections were measured and logged across the Los Choros Member:

1) LC section (informally named "Cerro Foraminifero"; base at 14°41′21.0″S, 75°37′40.0″W; top at 14°41′15.1″S, 75°37′39.9″W);
2) Ullujalla (ULA) section (informally named "Cerro Pata", and previously investigated by Morales et al., 2010, 2013; base at 14°39′57.9″S, 75°37′41.9″W; top at 14°39′47.7″S, 75°37′40.3″W);
3) PAN section (informally named "Cerro Panetón"; base at 14°42′41.3″S, 75°36′59.2″W; top at 14°42′36.6″S, 75°36′56.9″W);
4) GFL section (base: 14°38′28.7″S, 75°47′29.1″W; top: 14°38′42.7″S, 75°47′36.1″W) (Fig. 1). Measuring 46, 50, 80 and 7 m, respectively, these sections were logged using a high-precision Jacob's staff (Patacci, 2016). Despite widespread eolian sand cover, stratigraphic logging was conducted at a centimeter-to-decimeter scale where possible, including detailed descriptions of bed thickness, lithology, grain size (estimated with a grain-size comparator and hand lens), sedimentary structures, and bioturbation intensity. General facies analysis was also performed to integrate the measured sections into a broader stratigraphic and sedimentological framework (Di Celma et al., 2022). Thirty-five samples of coarse-grained (gravelly to sandy) material were collected from the Los Choros Member along the four measured sections. Six additional small outcrops (Fig. 1) were also surveyed and sampled (for a total of 6 additional samples of coarse-grained material). All coarse-grained rock samples were used for quantitative micropaleontological analysis, petrographic examination, and X-ray diffraction (XRD) analysis. Furthermore, to better constrain the age of the underlying shallow-marine deposits, fourteen samples were collected from the fine-grained deposits at the base of the overlying Yumaque Member and prepared for calcareous nannofossil biostratigraphy.

Measuring 46, 50, 80 and 7 m, respectively, these sections were logged using a high-precision Jacob's staff (Patacci, 2016). Despite widespread eolian sand cover, stratigraphic logging was conducted at a centimeter-to-decimeter scale where possible, including detailed descriptions of bed thickness, lithology, grain size (estimated with a grain-size comparator and hand lens), sedimentary structures, and bioturbation intensity. General facies analysis was also performed to integrate the measured sections into a broader stratigraphic and sedimentological framework (Di Celma et al., 2022). Thirty-five samples of coarse-grained (gravelly to sandy) material were collected from the Los Choros Member along the four measured sections. Six additional small outcrops (Fig. 1) were also surveyed and sampled (for a total of 6 additional samples of coarse-grained material). All coarse-grained rock samples were used for quantitative micropaleontological analysis, petrographic examination, and X-ray diffraction (XRD) analysis. Furthermore, to better constrain the age of the underlying shallow-marine deposits, fourteen samples were collected from the fine-grained deposits at the base of the overlying Yumaque Member and prepared for calcareous nannofossil biostratigraphy.

In addition to the samples collected along these newly examined sections and outcrops, nine samples of coarse-grained material collected at Zamaca (FOR section; base at 14°41′28.7″S, 75°36′50.1″W; top at 14°41′33.4″S, 75°36′57.4″W) and previously described in Coletti et al. (2019) were re-analyzed to perform detailed quantitative microfacies analysis.

3.2. Laboratory analyses

A bulk mineralogical characterization of the studied samples was assessed by means of XRD, using a PANalytical X'Pert PRO PW3040/60 diffractometer. Qualitative analysis was conducted based on the positions and relative intensities of the peaks in the XRD spectra. The latter were then compared with spectra of known compounds with the PANalytical X'Pert High-Score Plus® software, which allows for comparing between the measured 1/2θ profile and the standard 1/2θ profiles of pure phases from the International Centre for Diffraction Data. Quantitative analysis was undertaken with the Rietveld method (Rietveld, 1969), implementing the refinement of Gualtieri (2000) with the GSAS package (Larson and Von Dreele, 1994) and its graphical interface EXPGUI (Toby, 2001).

Samples for calcareous nannofossil analyses were prepared as standard smear slides (Bown and Young, 1998) and examined using an Olympus BX50 polarized light microscope at 1000× magnification with immersion oil at crossed nicols. Three longitudinal transects across the slide were analyzed to detect even rare marker taxa. The total abundance of calcareous nannofossils was estimated against the remaining components and the relative abundance of each species within the group was estimated per field of view (FOV) or transect on the slide, as: C = common; 5–10/FOV; F = few; 1/10 FOVs; R = rare; ≥3/transect; VR = 1/transect; B = barren. Preservation was estimated as good (G) if all the fine structures of the calcareous nannofossils were preserved; moderate (M) if the fine structures were affected by slight dissolution,

(caption on next page)

Fig. 2. Field photos of the studied Los Choros sections in the East Pisco Basin. A) Measured LC section at Cerro Foraminifero showing Los Choros strata. Note the alternation of consolidated coarser strata. B) Close up of a coarse layer enriched in internal and external molds of mollusks. C) Close up of the upper part of the LC section. D) Sampling site of LOSC samples (GFL section) along the way to Media Luna. E) Close up of a coarse layer of Figure D enriched in foraminifera. F) Contact between the basement and the Los Choros Fm at the FOR measured section (see also Coletti et al., 2019). G) Detail of Los Choros alternated strata at the locality of Media Luna. H) Measured PAN section at Cerro Panettone showing Los Choros strata. I) Panoramic view of Cerro Panettone showing Los Choros strata (left) and the basement (right). J) Measured ULA section at Cerro Pata. K) Close up of the alternation of Los Choros strata enriched in foraminifera. L) Close up of the contact between the basement and the Los Choros strata at the ULA section. M) Close up of a Los Choros layer enriched in foraminifera at the ULA section.

and bad (B) if only the central part of the nannofossils were preserved and the specific identification was prevented. Intermediate categories were also indicated. Calcareous nannofossil taxonomy and biochronology follow Agnini et al. (2014), Perch-Nielsen (1985) and Young et al. (2022). Full results on calcareous nannofossils are included in Supplementary Table S1.

Fifty thin sections were prepared at the Department of Earth and Environmental Sciences of Milano-Bicocca University following the procedure outlined by Coletti et al. (2025). The latter is based on three epoxy resin embedding cycles aimed at reinforcing the rock as well as at filling both the macro- and microporosity, which results in high-quality thin sections preserving fine morphological details of the microfossils. Quantitative microfacies analysis was based on both point counting (Flügel and Munnecke, 2010) and foraminiferal area counting (Mariani et al., 2024). Specifically, the skeletal assemblages and petrographic characteristics were analyzed using a 250 μm grid and counting more than 300 points in each section. The raw results of the skeletal assemblage analysis are included in Supplementary Table S2. The resulting data on the composition of the skeletal assemblages from the Pisco Basin were analyzed alongside a large dataset of middle Eocene skeletal assemblages from various sites in the Alpine and Dinaric foreland basins (Coletti et al., 2021a; Mariani et al., 2024) by means of ordination analysis. The latter is a robust tool for data interpretation that facilitates the investigation of datasets while minimizing a priori biases (Bialik et al., 2021). Through this method, similar objects are grouped together, while dissimilar objects are placed farther apart, thereby reducing the observed variability to a small number of components (Gauch and Whittaker, 1972; Syms, 2008; Bialik et al., 2021). Two different types of ordination analyses were employed: Non-metric MultiDimensional Scaling (NMDS) and Detrended Correspondence Analysis (DCA). NMDS generates an ordination replacing the original distance data with ranks, thereby avoiding issues associated with absolute distance (Kruskal, 1964). DCA is a variant of the correspondence analysis (Hill and Gauch Jr, 1980), which places the samples in the ordination space to maximize the correspondence, rather than the variance, between variables and data points. While standard correspondence analysis can be influenced by an "arch effect", this is corrected in DCA, making the latter better suited for portraying the relationships between variables. Both NMDS and DCA were performed using R software. Similarity was evaluated with the Bray-Curtis index (Bray and Curtis, 1957). To avoid issues related to uneven sample sizes and achieve a normal distribution of frequency data, the Hellinger transformation (i.e., the square root of the relative abundances) was applied (Legendre and Gallagher, 2001; Legendre and Borcard, 2018).

Foraminiferal assemblages were quantitatively assessed using the area counting method proposed by Mariani et al. (2024), which consists of identifying all the foraminifera in each thin section at the lowest taxonomically reasonable level, counting them, and referring their number to the surface area of the thin section itself for better comparisons with other samples. As large datasets are necessary for reliable paleoenvironmental reconstructions, there is a need for analyzing and comparing large numbers of samples. This requires practical taxonomic definitions that can be quickly and consistently used on large numbers of specimens, including those with sub-optimal orientation and preservation. With regards to low-trochospiral, biconvex, hyaline LBF of the superfamily Asterigerinoidea (mainly amphisteginids and asterigerinids), amphisteginids have been recognized based on the observation of the following characters: test involute, biconvex, poorly asymmetrical to almost symmetrical, without a thickened marginal cord, spacious alar prolongations, small (less than 100 μm in diameter) protoconch, and chambers strongly curved posteriorly towards the periphery (BouDagher-Fadel, 2018; Coletti et al., 2018a). Conversely, asterigerinids display a more planoconvex, asymmetrical outline of the test (e.g., Sirel and Deveciler, 2017; Benedetti et al., 2018). *Nummulites* species have a thicker marginal cord, narrower alar prolongations, a larger protoconch, chambers not strongly curved posteriorly towards the periphery, and a perfectly symmetrical outline of the test. Taxa within the family Rotaliidae exhibit tests that are either less symmetrical and/or more remarkably decorated (e.g., Hottinger and Bassi, 2014; Benedetti, 2015), therefore they cannot be confused with the other two groups. In anticipation of a comprehensive review of the American and Eurasian representatives of Lepidocyclinidae, we have elected to refrain from using subgenera, concentrating solely on the following genera: *Helicostegina*, *Helicolepidina*, *Polylepidina*, *Lepidocyclina*, *Nephrolepidina* and *Eulepidina*. *Helicostegina* is recognized as a lepidocyclinid lacking principal auxiliary chambers and displaying a well-defined main spire, with a thick spiral wall that is clearly observable throughout the test (Adams, 1987; BouDagher-Fadel and Price, 2010; Coletti et al., 2019). In turn, *Helicolepidina* is identified by a thinner wall of the main spire, resulting in a poorly recognizable spiral organization, especially towards the periphery of the equatorial plane (Adams, 1987; BouDagher-Fadel and Price, 2010; Coletti et al., 2019). *Polylepidina* is characterized by unequal principal auxiliary chambers giving rise to 2 to 4 nepionic spires of different lengths, thus resulting in a "botched" spiral organization that is only noticeable close to the embryo (Adams, 1987; BouDagher-Fadel and Price, 2010; Coletti et al., 2019). *Lepidocyclina* has instead equal to almost equal principal auxiliary chambers, and four equally developed nepionic spires; it is also characterized by a protonconch and a deuteroconch of roughly similar size, whereas in *Nephrolepidina* the protonconch is smaller than and partially embraced by the deuteroconch, and in *Eulepidina* the deuteroconch almost entirely embraces the protoconch (BouDagher-Fadel and Price, 2010; Coletti et al., 2019). The separation between *Lepidocyclina* and *Orbitoina* is based on the number of foramina/stolons connecting each chamber of the equatorial plane with adjacent chambers, this number being six in *Lepidocyclina* and four in *Orbitoina* (Van de Geyn and Van der Vlerk, 1935; Eames et al., 1962). This character can only be observed in well preserved, properly prepared oriented equatorial sections. Given that the aim of the present paper is paleoenvironmental, and considering also the poor preservation of most specimens, this trait could not be used and the notation *Lepidocyclina/Orbitoina* was applied instead. Although not free from issues, this approach represents the most effective means of classifying the thousands of foraminiferal specimens encountered in the studied samples in a comprehensive and consistent manner. Furthermore, this approach does not affect the paleoenvironmental interpretation of the investigated facies given the lack of detailed autecological information on the various groups clustered together by using the aforementioned criteria.

4. Results

4.1. Field observations

On the field (Fig. 2), the investigated sections (LC, ULA, FOR, PAN, and GFL) display broadly comparable vertical trends: very coarse-grained, siliciclastic-rich deposits at the base, overlain by alternating

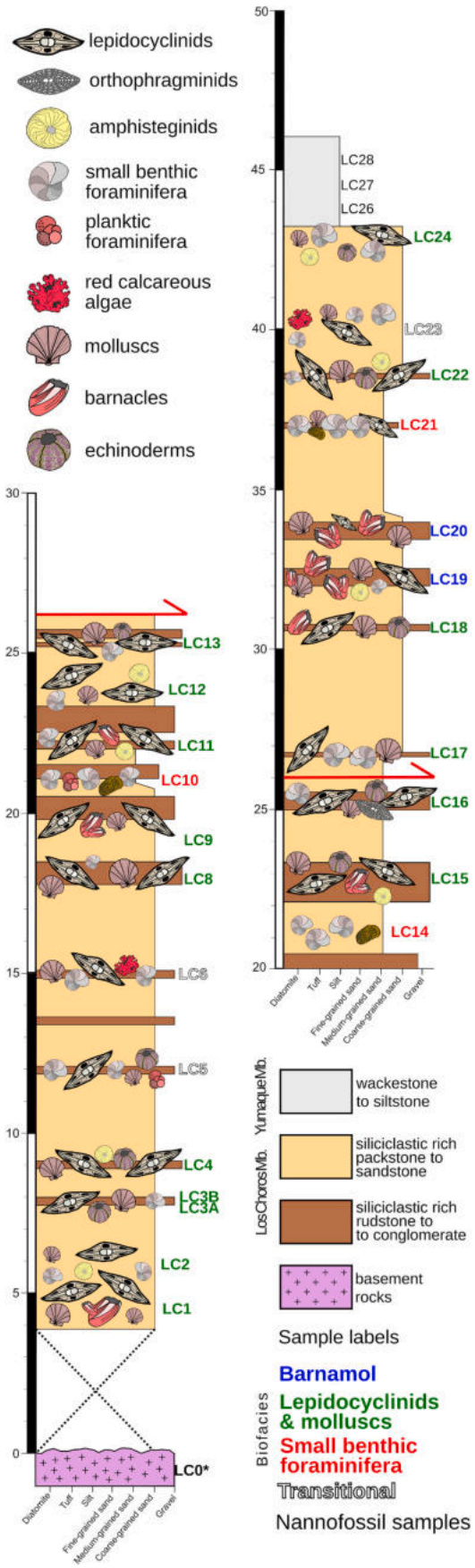

Fig. 3. Schematic stratigraphic log of the LC section. The log is divided into two parts to account for the small transfer fault.

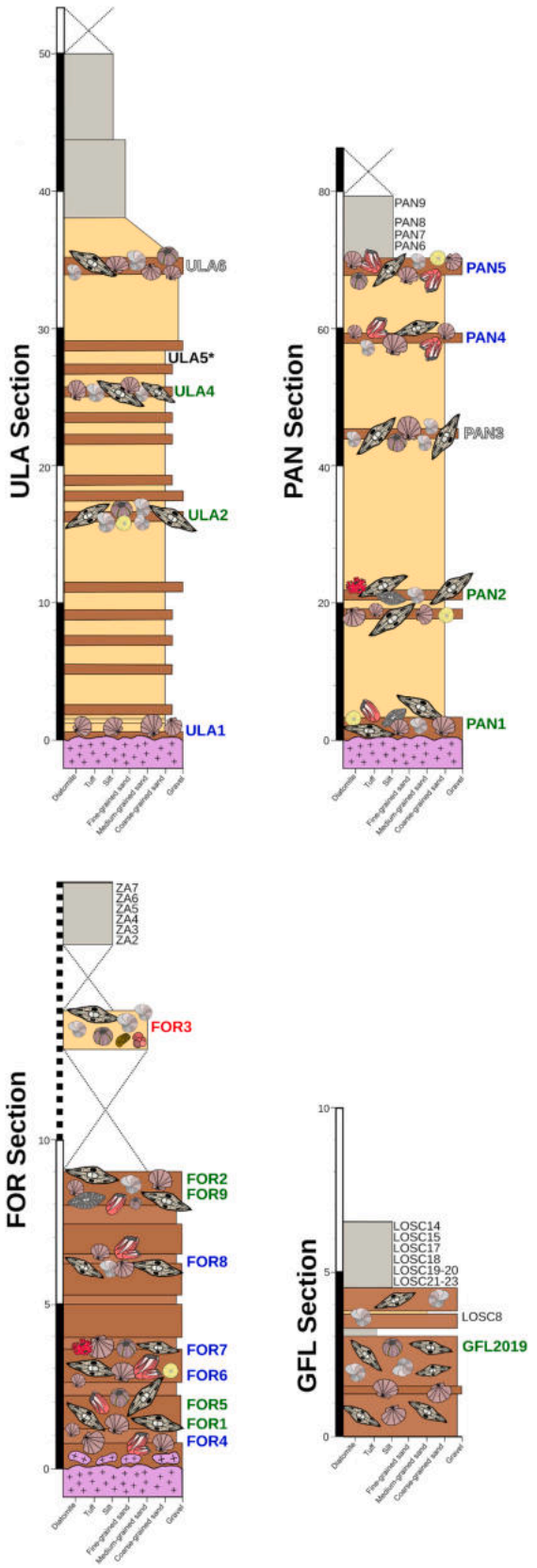

Fig. 4. Schematic stratigraphic logs of the ULA, PAN, FOR and GFL sections, note that the sections, given their variable length, are not represented using the same scale. The symbols are the same as in Fig. 3.

layers of coarse-grained and fine-grained, mixed siliciclastic-carbonate deposits. These coarse-grained strata are further overlain by the finer-grained, carbonate-rich deposits of the Yumaque Member.

The LC section (Fig. 2A–C), the longest and most complete of the investigated sections, consists of two contiguous sub-sections separated from each other by a small displacement normal fault (Fig. 3). The lower portion of the section directly overlies the crystalline basement rocks, but the nonconformity itself is hidden by modern eolian sand. The section is composed of coarse-grained beds with abundant LBF and mollusks alternating with more sandy intervals. The latter are often poorly exposed, which may be due to their greater compliance with weathering and erosion. Bioclasts generally display a weak preferred orientation. LBF usually dominate the visible skeletal assemblage. Barnacle wall plates, oysters, and other bivalves are also common, mostly occurring as disarticulated elements. Towards the top of the section, finer-grained beds become more frequent, transitioning progressively into the overlying, silt-prone Yumaque Member.

The ULA section (Fig. 2J–M), previously described by Morales et al. (2010, 2013), exhibits an overall vertical pattern similar to that of the LC section, with the Los Choros strata directly overlaying the basement rocks (Fig. 4). It features a basal interval of coarse-grained, siliciclastic-rich deposits dominated by mollusks (mostly oysters) followed upsection by LBF-rich beds. Echinoids are the only other fossils to be easily observed on the field. The skeletal material is usually randomly oriented, with local accumulations of disarticulated valves, especially along the basal nonconformity. Further upsection, thin gravelly layers alternate with thick sandy ones, both relatively poor in macrofossils. A bioturbated microconglomerate that fines upwards into the monotonous siltstones of the Yumaque Member further overlies these beds. Overall, compared to the other investigated sections and outcrops, the ULA section is richer in siliciclastic material and less obviously fossiliferous, especially towards the top.

The FOR section (Fig. 2F), previously described by Coletti et al. (2019), similarly to the other sections, rests directly onto the crystalline basement, and its lower and middle parts are dominated by coarse-grained deposits rich in LBF, mollusks and, to a lesser extent, barnacles (Fig. 4). Rare echinoderms, bryozoans and red calcareous algae are also present. Angular to sub-angular pebble-to boulder-sized clasts of rocks from the crystalline basement concentrate at the base of the succession. Upsection, coarse-grained siliciclastic elements become increasingly rarer, marking a shift to more strongly carbonate-dominated deposits. Further above, a siliciclastic-rich packstone occurs, being separated from the aforementioned strata by several meters of modern eolian sands. Once again, accumulations of wind-blown sand hide the vertical transitions of this packstone into the overlying, fine-grained deposits of the Yumaque Member.

The PAN section (Fig. 2H and I) consists of thick strata dominated by coarse-grained, mainly bioclastic deposits with abundant LBF and mollusks (Fig. 4). Along the section, layers rich in barnacles also occur, being associated with subordinate echinoderms, bryozoans and rare red calcareous algae. Further upsection, the silty Yumaque Member is found.

The GFL (Fig. 2D and E) section consists at the base of ca. 1.5 m of coarse-grained beds with no evident LBF, overlain by a layer of mollusk accumulation, especially bivalves, with both articulated and disarticulated shells (Fig. 4). The overlying 3 m are characterized by a great abundance of LBF, especially up to 3 m ab (above the base of the section), with two fine-grained layers intercalated in the coarse-grained succession of the Los Choros Member, possibly consisting of badly preserved volcanic ash layers (Fig. 4). The top of the succession consists of ca. 2 m of fine-grained sediments of the Yumaque Member, enriched in fish scales.

In addition to the stratigraphically constrained samples collected along the LC, ULA, FOR, PAN and GFL sections, six smaller, scattered outcrops of the Los Choros Member were also investigated (see their distribution in Fig. 1; Fig. 2G). Although frequently limited in terms of thickness and lateral continuity, these isolated exposures have yielded rich fossil assemblages comparable to those identified in the more continuous sections. This supports the consistency of the recognized biofacies across the investigated outcrop belt (Table 1). Indeed, the deposits of the scattered outcrops consist of coarse-grained, mixed siliciclastic-carbonate sediments, characterized by alternating well-cemented bioclastic beds and less cemented intervals. Field observations reveal that the observable coarse-grained fraction is consistently dominated by LBF and mollusks (including oysters and other recrystallized bivalves), associated with barnacles and rare echinoderms.

Table 1
Major petrographic characteristics, skeletal and foraminiferal assemblages of the investigated sites.

Sites	FOR	LC	PAN	ULA	GFL + scattered outcrops
Mineralogical composition (QXRD)					
Silicates	27.5	40.0	–	60.0	24.5
Carbonates	72.0	58.5	–	23.5	45.0
Texture (% point counting)					
Interstitial fraction	20.0	28.5	30.5	18.5	26.5
Siliciclastic fraction	23.5	30.0	27.0	44.5	21.0
Bioclastic fraction	56.5	42.5	42.5	37.0	52.5
Skeletal assemblage (% point counting)					
Red calcareous algae	2.0	0.5	1	0	0
LBF	46.0	45.0	34.0	30.5	55.0
Encrusting benthic foraminifera	0.5	0.0	0.5	0.0	0.0
SBF	8.5	21.5	16.5	22.0	9.5
Planktic foraminifera	0.5	0.0	0.0	0.0	0.0
Mollusks	30	18.5	31.5	40.0	22.5
Barnacles	8.5	8.5	11.0	0.0	9.0
Echinoderms	3.5	4.5	4.0	6.0	3.0
Bryozoans	0.0	0.5	0.5	0.0	0.5
Other heterotrophs	0.5	1.0	1.0	1.5	0.5
Foraminiferal assemblage (specimens in 1 cm^2)					
Lepidocyclinids	5.65	6.30	5.55	0.65	2.60
Orthophragminids	0.20	0.10	0.70	0.00	0.30
Amphisteginids	0.65	1.35	1.60	0.15	1.05
Hyaline SBF	1.15	2.05	19.95	0.15	0.30
Porcelaneous SBF	0.30	0.50	0.35	0.00	0.25
Agglutinated SBF	0.55	0.25	0.35	0.05	0.10

Table 2
Major petrographic characteristics, skeletal and foraminiferal assemblages of the recognized biofacies.

Biofacies	Barnamol	Lepidocyclinids and mollusks	SBF
Mineralogical composition (QXRD)			
Silicates	42.0	40.0	34.0
Carbonates	51.5	58.5	68.5
Texture (% point counting)			
Interstitial fraction	22.0	22.5	56.0
Siliciclastic fraction	37.0	26.5	13.0
Bioclastic fraction	41.0	51.0	31.0
Skeletal assemblage (% point counting)			
Red calcareous algae	1.5	0.5	0.0
LBF	21.5	60	15.0
Encrusting benthic foraminifera	0.5	0.5	0.0
SBF	3.0	9.5	73.0
Planktic foraminifera	0.0	0.0	1.5
Mollusks	51.0	18.0	1.5
Barnacles	20.0	7.0	0.0
Echinoderms	2.0	3.5	5.0
Bryozoans	0.0	0.5	0.0
Other heterotrophs	0.5	0.5	4.0
Foraminiferal assemblage (specimens in 1 cm^2)			
Lepidocyclinids	3.75	6.20	5.80
Orthophragminids	0.05	0.30	0.10
Amphisteginids	1.05	1.25	0.45
Hyaline SBF	1.50	2.85	6.70
Porcelaneous SBF	0.05	0.25	1.05
Agglutinated SBF	0.05	0.05	3.25

4.2. Biofacies

The microfacies analysis of the skeletal and foraminiferal assemblages allowed us to recognize three main biofacies (Table 2) – namely, the "barnamol", "lepidocyclinids-and-mollusks" and "SBF" (small benthic foraminifera) biofacies.

The barnamol biofacies characterizes coarse-grained (coarse sand-to granule-sized elements, with limited amounts of sub-sand-sized elements), siliciclastic-rich (between 1/3 and 4/5 of the bulk rock consists of siliciclastic terrigenous grains) deposits (Fig. 5A). Bioclasts often display a preferred orientation (Fig. 5B), are moderately to poorly sorted, and can display rounded edges (Fig. 5C). Terrigenous grains are typically coarse-sand-sized and angular. Rare, very poorly rounded grains have also been found (Fig. 5C). This biofacies characterizes the base and most of the FOR section. It also occurs at the base of the ULA section, in the upper part of the LC section and in the upper part of the PAN section, as well as in one of the scattered small outcrops. The skeletal assemblage is largely dominated by mollusks (usually dominant and mainly represented by oysters, pectinids and other recrystallized bivalves; Fig. 5A–D) and acorn barnacles (less frequently dominant and represented by disarticulated wall plates of archaic taxa lacking parietal tubes; Fig. 5E and F). Other common bioclasts are hyaline LBF (Fig. 5G), whereas small benthic foraminifera (hereinafter, SBF), red calcareous algae (Fig. 5D) and echinoderms are rare. Some encrusting benthic foraminifera (EBF) were also very rarely observed. Based on area counting data, the foraminiferal assemblage is largely dominated by lepidocyclinids (mainly *Lepidocyclina/Orbitoina*; Fig. 5G and H), associated with common hyaline SBF and amphisteginid LBF (Fig. 5I). Very rare orthophragmines, small miliolids and textulariids also occur.

The lepidocyclinids-and-mollusks biofacies consists of coarse-grained (coarse sand-to granule-sized elements with limited amounts of mud-sized material, except for the PAN section), siliciclastic-rich deposits (between 1/3 and 2/3 of the bulk rock consists of siliciclastic terrigenous grains) (Fig. 6A and B). Terrigenous grains are normally coarse-sand-sized and angular, but they can also be poorly rounded to rounded (Fig. 6A); smaller, fine-sand-sized grains are always angular. Bioclasts are usually moderately sorted and display a preferred orientation (Fig. 6B and C). Some bioclasts, barnacles and mollusks in particular, have rounded edges and exhibit evidence of abrasion (Fig. 6C). This biofacies occurs in all the studied sections and characterizes most of the LC section and the base of the PAN section. It also occurs in all but one of the scattered outcrops. The skeletal assemblage is mainly comprised of hyaline LBF associated with common mollusks (mainly oysters, pectinids and other recrystallized bivalves; Fig. 6D) and

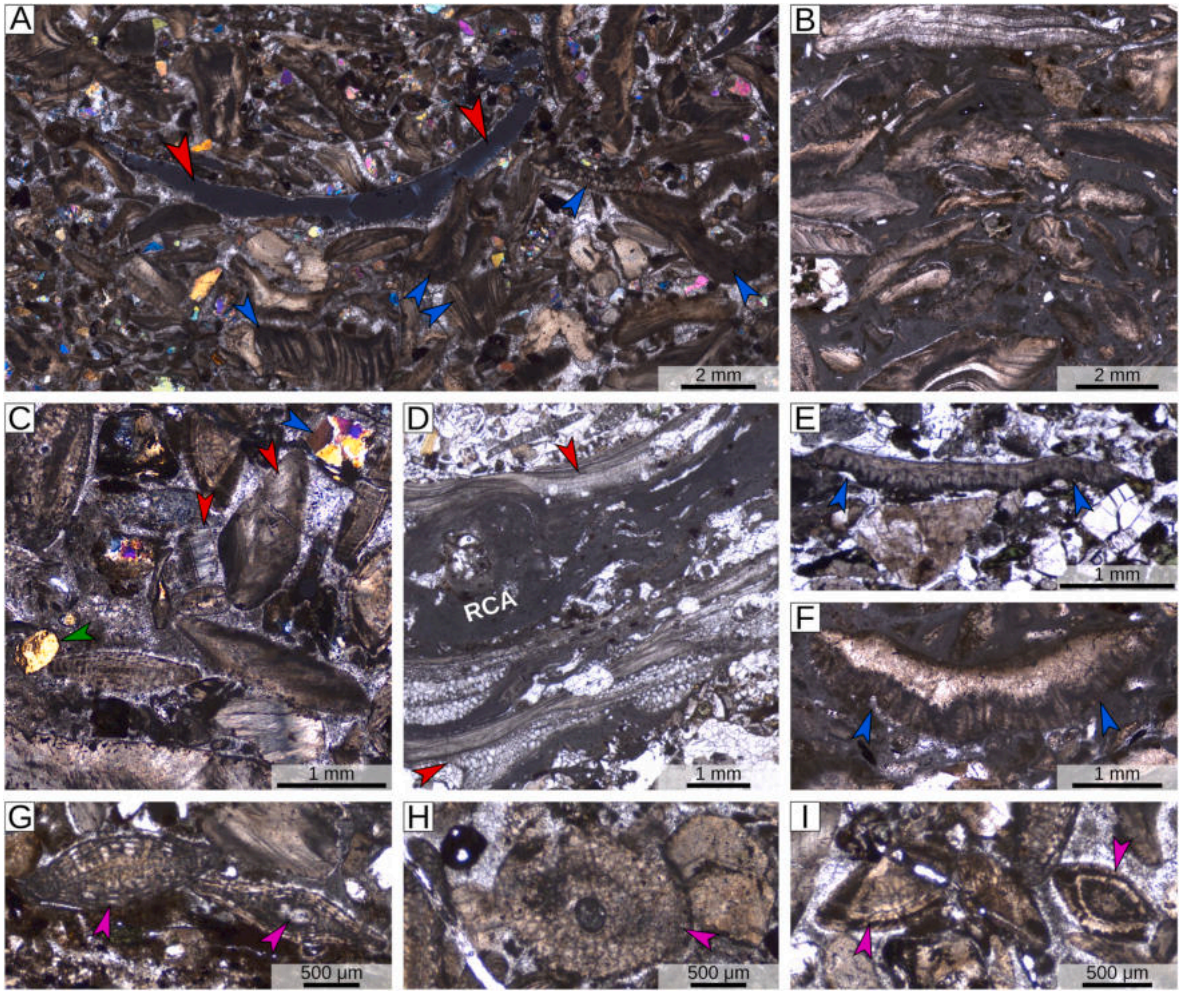

Fig. 5. Barnamol biofacies. A) LC section (LC20), biofacies overview (crossed polarizer), red arrowheads = recrystallized mollusk, blue arrowheads = barnacles. B) Small outcrop (G5), skeletal grains displaying common orientation. C) LC section (LC19), rounded bioclastic and siliciclastic grains; red arrowheads = rounded bioclastic grains, green arrowhead = rounded terrigenous grain; blue arrowhead = angular terrigenous grain. D) FOR section (FOR7), large oyster fragment (red arrowheads), encrusted by a red calcareous alga (RCA). E) FOR section (FOR7), acorn barnacle plate (blue arrowheads). F) Scattered outcrop (G5), acorn barnacle plate (blue arrowheads). G) LC section (LC19), axial section of lepidocyclinids, pink arrowheads = equatorial plane of the LBF. H) LC section (LC19), nearly equatorial section of a lepidocyclinid, pink arrowhead = poorly preserved equatorial chamberlets. I) LC section (LC19), amphisteginids (pink arrowheads). (For interpretation of the references to colour in this figure legend, the reader is referred to the Web version of this article.)

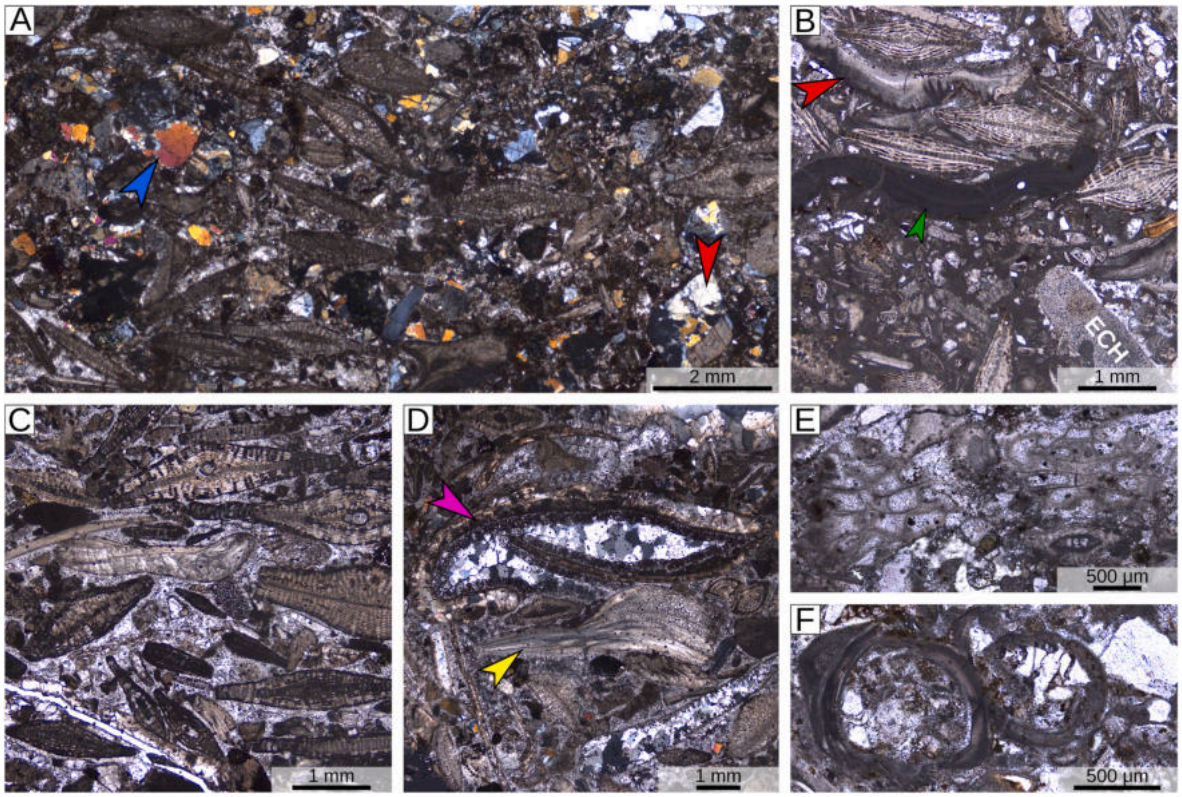

Fig. 6. Lepidocyclinids and mollusks biofacies. A) LC section (LC4), overview of the biofacies (crossed polarizer), blu arrowhead = angular terrigenous grain, red arrowhead = rounded terrigenous grain. B) PAN section (PAN2), sample displaying the lepidocyclind and mollusk biofacies rich in fine-grained matrix and displaying preferential orientation of the grains, ECH = echinoderm fragment, red arrowhead = acorn barnacle plate, green arrowhead = red calcareous alga. C) LC section (LC2), skeletal grains displaying common orientation. D) LC section (LC9), recrystallized mollusk shell (pink arrowheads) and an oyster fragment (yellow arrowhead). E) Small outcrop (G4), bryozoans. F) PAN section (PAN2), serpulids. (For interpretation of the references to colour in this figure legend, the reader is referred to the Web version of this article.)

SBF. Scarce acorn barnacles, rare echinoderms, very rare red calcareous algae (Fig. 6B), bryozoans (Fig. 6E), serpulids (Fig. 6F), and extremely rare, poorly preserved, planktic foraminifera also occur. The foraminiferal assemblage is dominated by lepidocyclinids (mainly *Lepidocyclina/Orbitoina*) (Fig. 7A–C), associated with abundant hyaline SBF (mainly belonging to the Cibicididae family) (Fig. 7C–E). Common amphisteginids (7F, G), and rare orthophragminids (Fig. 7C and D), textulariids, and small miliolids also occur (Fig. 7H and I). The latter are mostly found in the PAN section, where the overall abundance of SBF is much higher than in the other sections.

The SBF biofacies characterizes sandy layers occurring either as interbeds among the coarse-grained layers of the aforementioned biofacies (e.g., along the LC section), or close to the top of the investigated sections (e.g., FOR section). The terrigenous fraction mainly consists of fine-sand-sized angular grains (Fig. 8A). Bioclasts are poorly sorted, ranging from fine sand-sized SBF to granule-sized lepidocyclinid tests, and usually lack a preferred orientation (Fig. 8A–C). This biofacies is mainly recorded at the top of the FOR section, and in the middle and upper parts of the LC section. It was not observed in the smaller outcrops. The bulk mineralogical composition is dominated by carbonates, with siliciclastic terrigenous materials accounting from around 10% up to half of the bulk rock. The skeletal assemblage is dominated by SBF (Fig. 8B and C) associated with common LBF, scarce echinoderms, and rare mollusks (mainly bivalves), ostracods and poorly preserved planktic foraminifera. The foraminiferal assemblage is dominated by hyaline SBF (mainly belonging to the families Bolivinitidae, Nonionidae and, more rarely, Stilostomellidae; Fig. 8B and C) associated with abundant lepidocyclinids (mainly *Lepidocyclina/Orbitoina*), common small textulariids, planktic foraminifera and small miliolids, and rare amphisteginids. Very rare orthophragminids also occur.

In addition to these three main biofacies, samples characterized by transitional assemblages were also observed (Fig. 8D and E).

4.3. Biostratigraphy

LBF assemblages from the examined samples are dominated by small lepidocyclinids characterized by a small isolepidine embryo, i.e., they display a protoconch and a deuteroconch of similar size (Fig. 9A–C). These initial chambers are separated by a straight wall (i.e., the deuteroconch does not embrace the protoconch, Fig. 9A–C) and they are surrounded by relatively large periembryonic chambers, including large, asymmetrical, principal auxiliary chambers (Fig. 9A–C). Previous biometric analyses (Coletti et al., 2019) identified these specimens as *Lepidocyclina rdouvillei* Lisson (1921), which has subsequently recombined as *Orbitoina rdouvillei* by Mitchell et al. (2022). This taxon is associated with rare specimens of more archaic lepidocyclinids exhibiting a distinct single-spire organization of the equatorial plane (Fig. 9D–F). These specimens are poorly preserved, making an accurate identification impossible; however, the comparatively long spire suggests a placement within *Helicostegina* or *Helicolepidina* (or some other comparable genera) (Fig. 9D and E). Coletti et al. (2019) also recorded the presence of the genus *Polylepidina*.

Based on the co-occurrence of basal representatives of *Orbitoina/Lepidocyclina* and archaic lepidocyclinids characterized by a single main spire on the equatorial plane, the examined strata of the Los Choros Member can be assigned to the American Benthic Zones (ABZ) 10 or 11 (Mitchell et al., 2022, 2024). The latter corresponds to the central part of plankton zone P12, which should span from 43.6 to 40.5 Ma (i.e., late Lutetian to earliest Bartonian) based on Wade et al. (2011) calibration.

In the analyzed sections (LC, ULA, PAN, and GFL), nannofossil

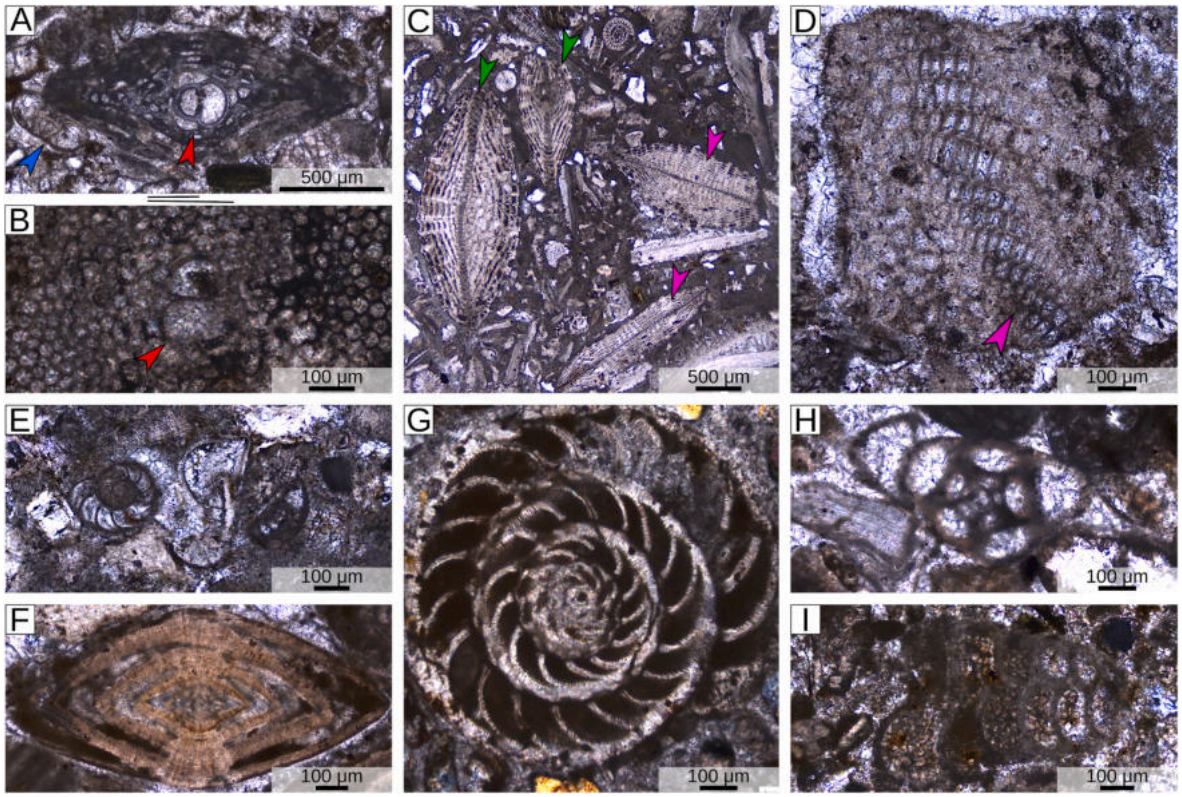

Fig. 7. Foraminiferal assemblage of the lepidocyclinids and mollusks biofacies. A) LC section (LC22), axial section of a *Lepidocyclina/Orbitoina*, red arrowhead = embryonic chambers, blue arrowhead = small hyaline benthic foraminifera. B) LC section (LC9), equatorial section of a *Lepidocyclina/Orbitoina*, red arrowhead = protoconch. C) PAN section (PAN2), axial sections of lepidocyclinids and orthophragmines showcasing the difference in the thickness of the equatorial plane, green arrowheads = lepidocyclinids, pink arrowhead = orthophragminid. D) PAN section (PAN1), orthophragminid fragment displaying the rectangular shape of the equatorial chambers (pink arrowhead). E) PAN section (PAN2), hyaline small benthic foraminifera. F) Small outcrop (MED19), transitional biofacies (lepidocyclinids and mollusks and SBF biofacies), amphisteginid, axial section. G) LC section (LC24), equatorial section of an amphisteginid, notice the chambers strongly curved posteriorly towards the periphery and the small protoconch. H) Small outcrop (G3), small miliolid. I) LC section (LC6), transitional biofacies (lepidocyclinids and mollusks and SBF biofacies), small agglutinated benthic foraminifera, possibly *Textularia*. (For interpretation of the references to colour in this figure legend, the reader is referred to the Web version of this article.)

assemblages from the portion of the Yumaque Member directly overlying Los Choros (Fig. 10) show a typical middle Eocene assemblage dominated by different species of *Reticulofenestra* and *Coccolithus*, except for ULA samples that are barren. Zonal markers recovered at all sections include *Reticulofenestra umbilicus* (Base 43.03 Ma, Top 32.02 Ma, Agnini et al., 2014), *Reticulofenestra reticulata* (Base 42.37 Ma, Top 35.24 Ma, Agnini et al., 2014), and *Discoaster saipanensis* (Base 46.29–49.11 Ma, Young et al., 2022; Top 34.44 Ma, Agnini et al., 2014). *Sphenolithus furcatulithoides* (Base 45.95 Ma - Top 40.34 Ma) was recovered in most samples from the GFL section, while *Reticulofenestra bisecta* (Base 40.4 Ma, Agnini et al., 2014) was found in the two uppermost PAN samples. Additional species of biostratigraphic importance recovered in the analyzed sections include *Chiasmolithus solitus* (Base 55.86–57.21 Ma, (Young et al., 2022); Top 39.8–38.7 Ma, Agnini et al., 2014), *Sphenolithus spiniger* (Base 46.29–49.11Ma, Perch-Nielsen, 1985, Top 37.32–40.40 Ma, Fornaciari et al., 2010) and middle-late Eocene *Helicosphaera* species (*H. compacta*, *H. reticulata*). The age of the basal Yumaque strata in these sections is therefore constrained between 42.37 Ma and 40.4 Ma (between the Base of *R. reticulata* and the base of *R. bisecta*). The first occurrence of *R. bisecta* is documented only in the highest samples of the PAN section but not along the LC and ULA sections. The LC section continues into the MB section studied by Malinverno et al. (2021), where the FO of *R. bisecta* is documented. The same age range, based on nannofossil assemblages, was also inferred for the FOR section analyzed in Coletti et al. (2019).

Overall, the LBF assemblage, together with the calcareous nannofossil assemblage of the base of the Yumaque Member, constrains the deposition of the Los Choros Member during the early late Lutetian, at around 43 Ma (likely later than 43.6 and before 42.37).

4.4. South American versus European middle Eocene shallow-water carbonate systems

The ordination analysis of the quantitative skeletal assemblage data enables a broad comparison between the middle Eocene shallow-marine sediments of the Pisco Basin and those from the Alpine and Dinaric foreland basins. The Alpine foreland basin is represented by four sites distributed across its southwestern sector, while the Dinaric foreland basin is represented by an additional site.

The NMDS space features (1) an upper central sector with samples rich in authotrophs (red and green calcareous algae) and mixotrophs (LBF) carbonate producers; (2) a lower left corner characterized by samples rich in mollusks and sessile benthic filter feeders (mainly bryozoans and barnacles); and (3) a lower right sector with samples rich in planktic foraminifera and other carbonate producers (mainly ostracods) related to outer shelf settings. Samples from the investigated Peruvian sections and the scattered outcrops largely overlap with each other, indicating no major variations in the skeletal assemblages (Fig. 11). Taken together, South American samples predominantly occur within the sector defined by abundant heterotrophs, but they also display a large overlap with the clusters encompassing the European samples (Fig. 11). The DCA analysis, which excludes LBF as a variable given their limited contribution to the system overall variability as highlighted by the NMDS, displays a nearly identical pattern (i.e.,

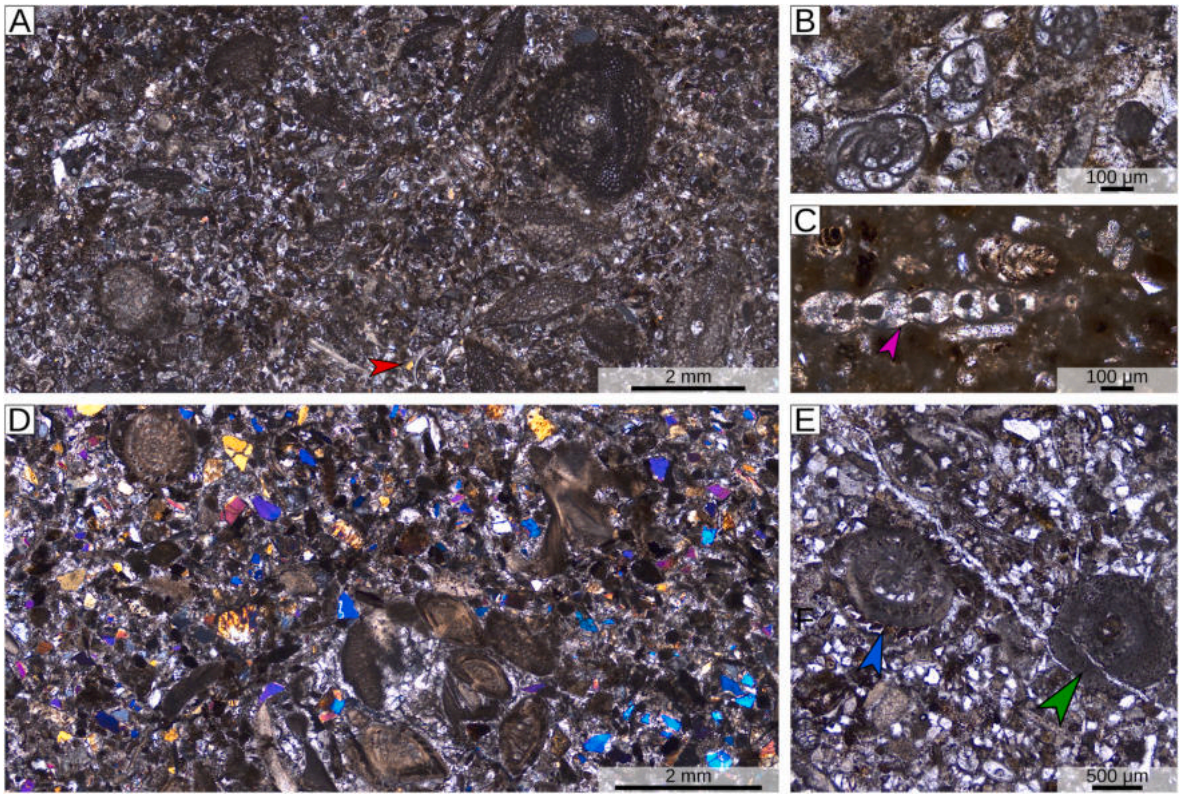

Fig. 8. SBF biofacies. A) FOR section (FOR3), overview (crossed polarizer) of the facies and its texture, red arrowhead = terrigenous grain. B) FOR section (FOR3), nonionids. C) LC section (LC14), small hyaline benthic foraminifera, pink arrowhead = *Stilostomella*. D) Small outcrop (MED19), transitional biofacies (lepidocyclinids and mollusks and SBF biofacies), overview of the sample and its texture (crossed polarizer), notice the angular terrigenous grains. E) PAN section (PAN3), transitional biofacies (lepidocyclinids and mollusks and SBF biofacies), large benthic foraminifera, blue arrowhead = amphisteginid, green arrowhead = lepidocyclinid (possibly *Helicolepidina*). (For interpretation of the references to colour in this figure legend, the reader is referred to the Web version of this article.)

vectors related to phototroph and mixotroph carbonate producers diverge from those related to heterotroph carbonate producers) (Fig. 12). Calcareous algae and encrusting benthic foraminifera vectors are at high angle with planktic foraminifera and green calcareous algae vector is at high angle with the mollusk and sessile benthic filter feeders' vectors. Similar to the NMDS, also in the DCA there is an almost complete overlap between the different sub-sets of samples from the Pisco Basin as well as a significant overlap between these samples and those from the Eurasian basins. However, much like in the NMDS, South American samples clearly show an overall higher abundance of heterotroph carbonate producers.

5. Discussion

5.1. Paleoenvironmental reconstructions

The studied biogenic skeletal grains of the Los Choros Member display some evidence of reworking (e.g., rounded edges of bioclasts) and dissolution (e.g., the occurrence of moldic porosity as well as the limited number and poor preservation of red calcareous algae and porcelaneous foraminifera). Although this advises against the use of highly detailed proxies based on the composition of the coralline algal flora and foraminiferal fauna, the available quantitative data on the skeletal and foraminiferal assemblages, combined with field observations, enable us to develop hypotheses about the depositional paleoenvironment of the Los Choros Member.

With respect to the barnamol biofacies, the abundance of barnacles suggests a shallow-water coastal setting. Most modern acorn barnacle-rich facies occur in high-energy environments bordered by rocky coasts where barnacles can settle in large numbers, at water depths of less than 50 m (most typically <15–20 m) (Coletti et al., 2018b). High-energy conditions are also supported by barnacle taphonomy as barnacles are entirely represented by disarticulated and invariably rounded wall plates (Fig. 5C) (Coletti et al., 2024; Bosio et al., 2025b). This interpretation is consistent with the remainder of the skeletal assemblage (including light-dependent carbonate producers such as LBF), the relevant siliciclastic fraction, and the common orientation of the skeletal grains. However, additional elements must be considered. First and foremost, Paleogene barnacle-rich facies are uncommon (e.g., Donovan, 1993; Buckeridge et al., 2014), and our paleoenvironmental understanding of this skeletal assemblage is essentially based on Neogene and Quaternary occurrences (Coletti et al., 2018b). This suggests some caution in interpreting Paleogene barnacle-rich deposits based on patterns and processes of their geologically younger counterparts. Secondly, the abraded state and iso-orientation of the skeletal components suggest they underwent somewhat prolonged physical reworking on the seafloor prior to final burial. Physical reworking likely induced some mechanical selection of the bioclasts and potential mixing of invertebrate communities originating from different settings, further complicating the paleoenvironmental interpretation.

The dominance of LBF in the lepidocyclinids-and-mollusks biofacies reveals that its genesis must be searched for within the photic zone. The lower number of barnacles (Table 2) suggests a deeper formation environment compared to the barnamol facies. Lepidocyclinds are regarded as middle to outer shelf dwellers (Geel, 2000; BouDagher-Fadel, 2018; Mitchell et al., 2022), and lepidocyclinids-dominated facies are thought to form around 30–60 m water depth (Bosellini et al., 1987; Coletti et al., 2021b). However, these hypotheses are mainly based on the paleontological analysis of Oligocene and Miocene lepidocyclinid-rich facies from Eurasia, which may have been different from coeval facies from

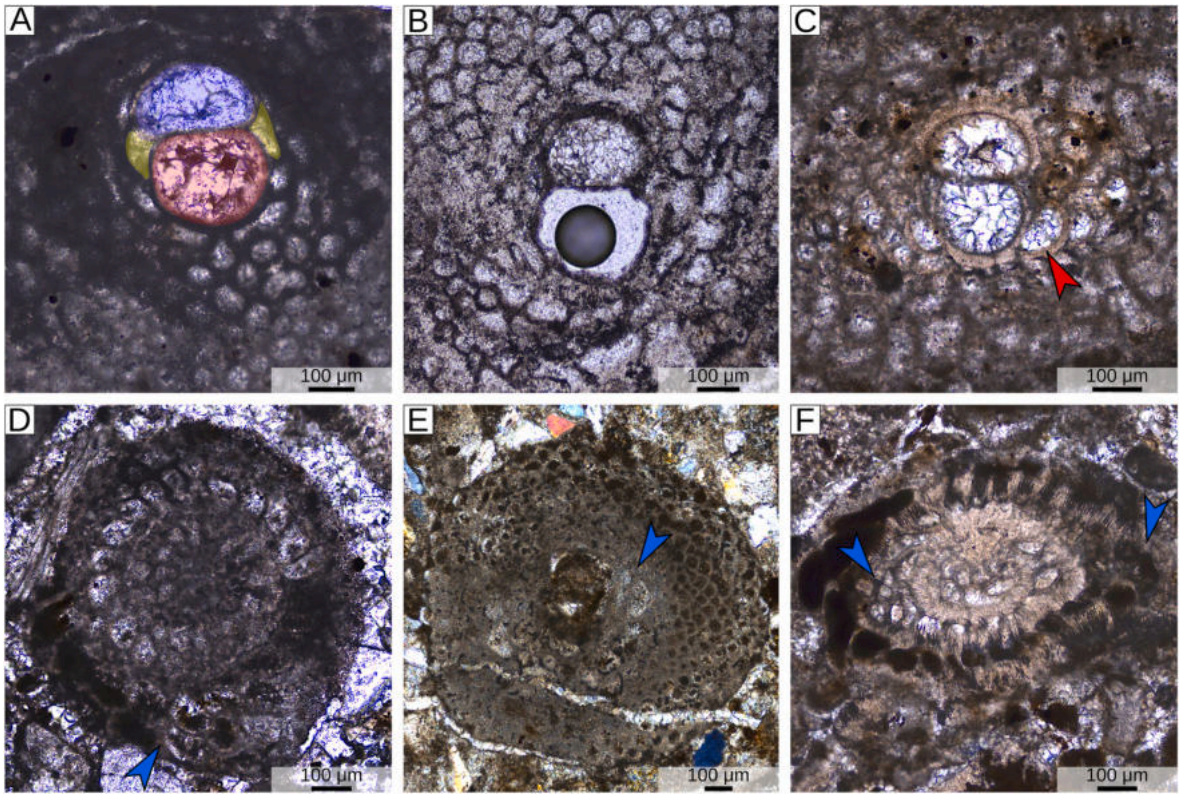

Fig. 9. LBF from the coarse-grained strata of the Los Choros Member. A) Small outcrop (G4), specimen of *Lepidocyclina/Orbitoina* displaying its isolepidine embryo (i.e. protoconch and deuteroconch of similar size) with large principal auxiliary chambers, red shading = protoconch, blue shading = deuteroconch, yellow shading = principal auxiliary chambers. B) LC section (LC4), specimen of *Lepidocyclina/Orbitoina* displaying its isolepidine embryo. C) LC section (LC5), specimen of *Lepidocyclina/Orbitoina* displaying its isolepidine embryo and its large peri-embryonic chambers (red arrowheads. D) LC section (LC1), lepidocyclinid specimen clearly displaying both the subdivision of the equatorial plane into chamberlets (blue arrowhead) and a spiral organization, the specimen probably belongs to genus *Helicostegina*. E) PAN section (PAN3), lepidocyclinid specimen displaying a spiral organization close to the embryo (blue arrowhead) and possibly belonging to the genus *Helicolepidina*. F) LC section (LC5), lepidocyclind specimen cut along a pseudo-axial section and displaying both a spiral organization and the division of chambers into chamberlets (blue arrowhead). (For interpretation of the references to colour in this figure legend, the reader is referred to the Web version of this article.)

South America. While this weakness cannot be completely dismissed, the distribution of orthophragminids may provide significant hints. Indeed, orthophragminids occur in both the lepidocyclinids-and-mollusks biofacies of the Los Choros Member, and in the middle Eocene carbonate systems of Eurasia, where they have been thoroughly investigated for biostratigraphic and paleoenvironmental purposes (e.g., Ćosović and Drobne, 1995; Less, 1998; Sinclair et al., 1998; Özcan et al., 2022). In Eurasian systems, the dominance of orthophragminids is regarded as suggestive of lower photic zone settings (e.g., Sinclair et al., 1998), which should correspond to water depths between 60 and 130 m under oligotrophic conditions (e.g., Coletti et al., 2021a). Orthophragminids can also be found, without being dominant, in shallower environments (40–60 m water depth, once again in oligotrophic conditions; e.g., Coletti et al., 2021a; Mariani et al., 2024). In view of these considerations, it is reasonable to infer that the lepidocyclinids-and-mollusks biofacies developed between the lower limit of the dominance of the barnamol biofacies and the upper limit of the lower photic zone, which in turn represents the upper limit of the orthophragminid dominance. The bathymetric range of these boundaries is determined by water transparency, and as such, it is deeper in sunlit oligotrophic water far from river mouths and coastal runoff, and shallower where nutrient and terrigenous supplies are relevant (e.g., Hallock and Schlager, 1986). The overall abundance and diversification of heterotrophs in the examined skeletal assemblages suggests that the Los Choros deposits formed in mesotrophic conditions (Hallock and Schlager, 1986; Bialik et al., 2023). Given that the Pisco Basin was located at a paleolatitude of approximately 19–20°S during the middle Eocene (Vaes et al., 2023), the light penetration model in a tropical upwelling system, such as modern Galapagos Islands, can be used as a reference. The Galapagos are influenced by seasonal and interannual upwelling of deep, nutrient-rich water, which results in increased primary production in surface water and, consequently, in increased concentrations of plankton and particulate organic carbon, reducing water transparency and the extent of the photic zone (Hallock and Schlager, 1986; Reymond et al., 2016). Based on the extension of the photic zone in the Galapagos (Faul et al., 2000), a water depth comprised between 15 and 40 m can be envisioned for the lepidocyclinids-and-mollusks facies of the Los Choros Member.

The SBF biofacies is dominated by small hyaline foraminifera of the families Bolivinitidae and Nonionidae associated with a sizable amount of lepidocyclinids and other hyaline LBF, some stilostomellids and poorly preserved planktic foraminifera. Bolivinitids and nonionids are often infaunal, can tolerate dysoxic conditions and occur over a wide depth range, from the inner shelf to bathyal settings (Murray, 2006). The elongate, uniserial, calcareous benthic foraminifera of the family Stilostomellidae are usually associated with deep-sea assemblages (Hayward, 2002). The presence of these hyaline SBF taxa, coupled with the reduced abundance of lepidocyclinids and amphisteginids as well as with the absence of barnacle fragments (Table 2), suggests that the SBF biofacies is related to a sandy-muddy seafloor slightly deeper than those hosting the barnamol and lepidocyclinids-and-mollusks biofacies. The overall scarce presence of planktic foraminifera indicates that the overlying water column was not particularly thick. Indeed, in the ordination space (Figs. 11 and 12), the Los Choros samples do not stretch

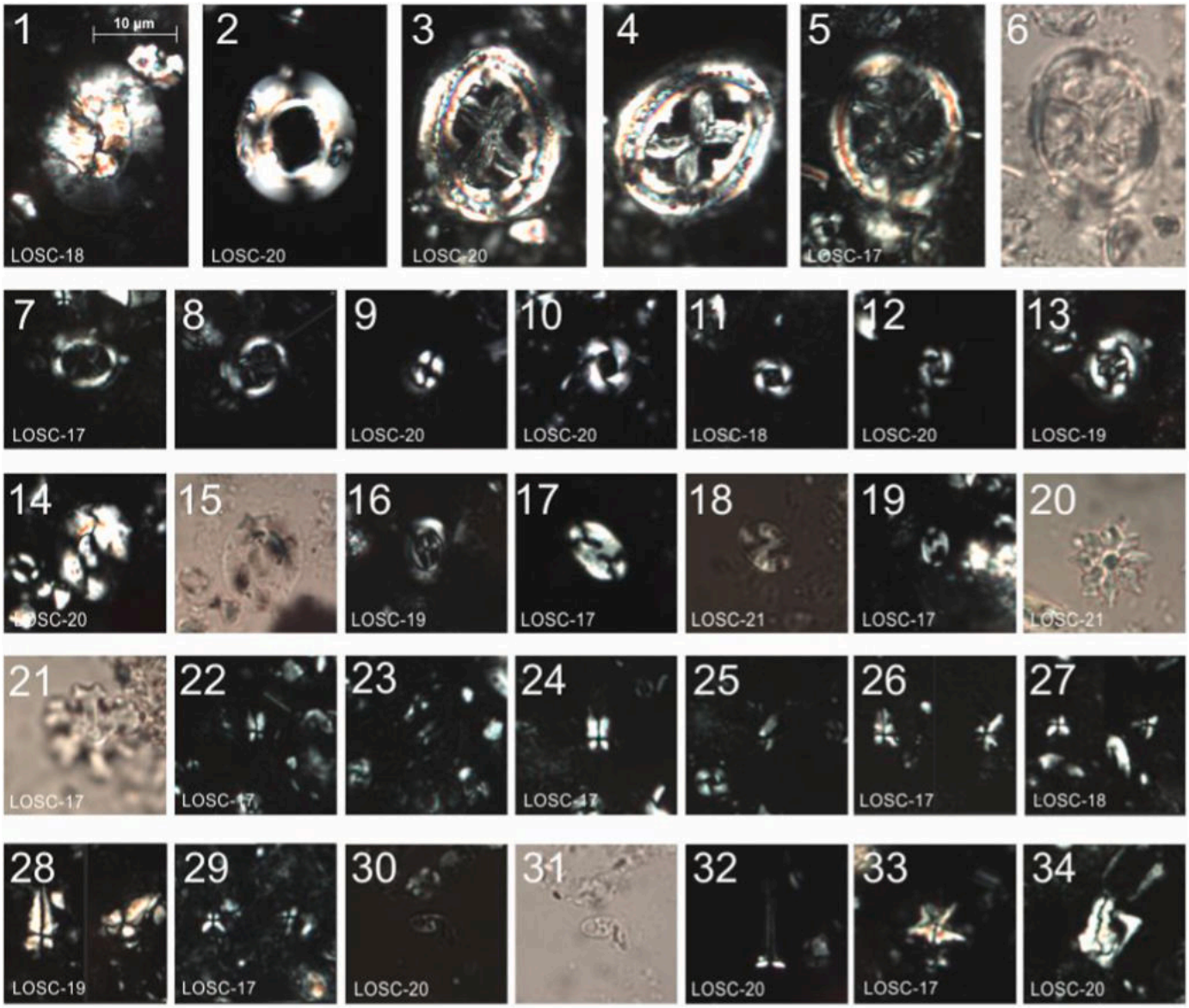

Fig. 10. Calcareous nannofossils from the analyzed samples at the base of the Yumaque member of the Paracas Formation, mainly from GFL section. 1) *Coccolithus eopelagicus*; 2) *Reticulofenestra pseudoumbilicus*. 3, 4) *Chiasmolithis grandis* at 90° and 45°. 5, 6) *Ch. expansus*, crossed and parallel nicols. 7, 8) *Ch. solitus*, 90° and 45°. 9) *C. pelagicus*. 10) *R. dictyoda*. 11) *R. reticulata*. 12) *R. daviesii*. 13) *Ch. titus*. 14; 15) *Helicosphaera lophota*. 16) *Campylosphaera dela*. 17) *Pontosphaera exilis*. 18) *P. pulcheroides*. 19) *P. pygmaea*. 20) *Discoaster saipanensis*. 21) *D. deflandrei*. 22, 23) *Sphenolithus furcatolithoides*. 24, 25) *S. furcatolithoides* B of Agnini et al. (2014). 26) *S. radians*. 27) *S. spiniger*. 28) *S. pseudoradians*. 29) *S. orphanknollensis*. 30, 31) *Neococcolithes minutus*. 32) *Blackites spinosus*. 33) *Micrantholithus astrum*. 34) *Zygrhablithus bijugatus*.

much along the planktic foraminifera axis compared to the European sites, which include samples associated with a water depth of more than 100 m (Coletti et al., 2021a; Mariani et al., 2024). Therefore, consistent with the relevant presence of LBF, a water depth only slightly higher than the barnamol and lepidocyclinids-and-mollusks biofacies is proposed for the SBF biofacies. The abundance of taxa potentially able to endure hypoxic conditions (e.g., nonionids) is also in agreement with the nutrient-rich conditions proposed on the basis of the relevance of heterotrophs in the other biofacies.

The lack of vertical trends in biofacies distribution and the presence of several samples reflecting transitional assemblages suggest a ramp profile with a homogeneous slope and relevant mixing of skeletal assemblages from contiguous environments. This mixing further questions the reliability of our water depth estimates, which should be thus regarded as approximate. Nonetheless, based on the terrigenous content of the studied samples, and considering the barnacle biofacies as the most proximal and the SBF biofacies as the most distal, a paleoenvironmental reconstruction of the study area during the deposition of the Los Choros Member is here attempted (Fig. 13). At that time, the Pisco Basin was probably characterized by an indented coastline, dissected by syndepositional normal faults with some footwall-related rocky islands and hangingwall-related embayments sheltering certain areas from the full force of storm waves. Within this context, the siliciclastic-dominated ULA section was probably located in an exposed location very close to basement rocky cliffs, whereas the more bioclastic-rich FOR and PAN sections were probably located in shallow embayments less close to the coast. The PAN section in particular, is the only section to display a relevant muddy fraction even in its coarse-grained bioclastic deposits, which suggests a relatively sheltered location. Most of this topography was likely drowned during the marine transgression testified by the overlying Yumaque Member.

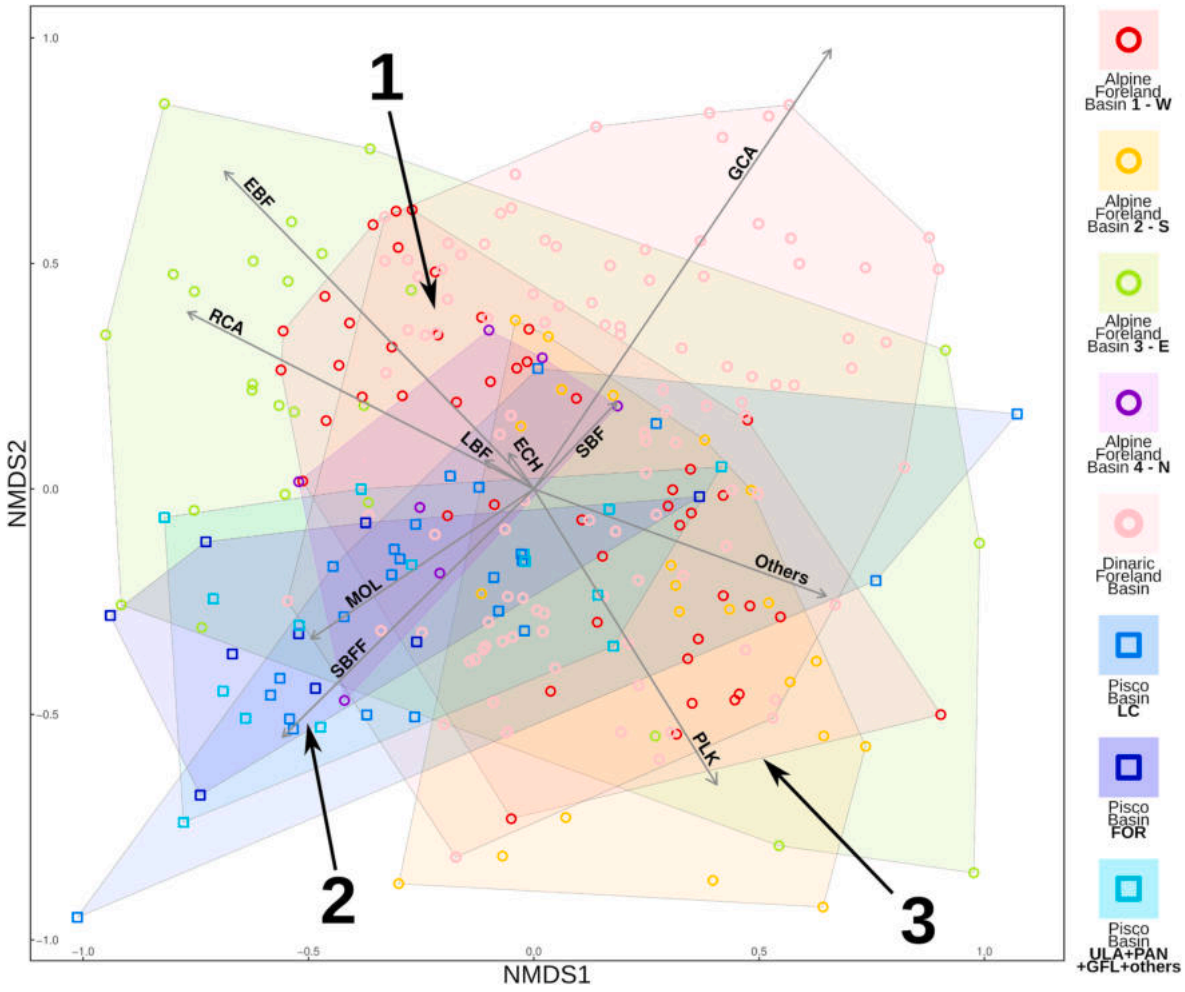

Fig. 11. NMDS plot of the skeletal assemblages of the various samples from the Pisco Basin (squares) and from Tethys (circles). The plot features an upper central sector with samples rich phototrophs = 1, a lower-left corner characterized by samples rich in heterotrophs = 2, a lower-right sector with samples rich in planktic foraminifera = 3. RCA = red calcareous algae, GCA = green calcareous algae, LBF = large benthic foraminifera, SBF = small benthic foraminifera, EBF = encrusting benthic foraminifera, PLK = planktic foraminifera, MOL = mollusks, ECH = echinoderms, SBFF = sessile benthic filter feeders (barnacles + serpulids + bryozoans + brachiopods), Other = other biogenic grains (mainly ostracods), W= West, S= South, E = East, N= North. (For interpretation of the references to colour in this figure legend, the reader is referred to the Web version of this article.)

5.2. Regional and global implications

The examined biogenic carbonates share remarkable similarities with their coeval Eurasian counterparts, the most prominent being that the photozoan component is dominated by LBF in both cases (Nebelsick et al., 2005; Coletti et al., 2022). While LBF dominance is not exclusive to the Eocene shallow-water carbonates of the Pisco Basin, as LBF-rich facies are documented across various other South and Central American localities (Aguilera et al., 2020, and references therein), this similarity indicates that, in both the American and Eurasian tropical bioprovinces, other light-dependent carbonate producers (e.g., symbiont-bearing colonial corals and calcareous algae) were outcompeted by LBF across much of the photic zone. This "gilded age" of the LBF has been attributed by Coletti et al. (2022) to the remarkably high global temperatures that characterized the early and middle Eocene (Westerhold et al., 2020).

Unlike many middle Eocene LBF-dominated facies from the Eurasian Tethys, those of the Pisco Basin contain a significant proportion of heterotrophs, suggesting higher nutrient availability and/or cooler conditions (Bialik et al., 2023) (Figs. 11 and 12). Nowadays, the Pisco Basin is located on the Pacific coast of South America, where the action of trade winds and Humboldt Current drives an intense coastal upwelling. During the middle Eocene, the study area was located only 5° south of its current position (Vaes et al., 2023), suggesting that the effect of trade winds may have been comparable to that of the present day. On the other hand, the Humboldt Current is not expected to have been fully established, at least not with its modern intensity. The sustained thermohaline circulation that currently drives the Humboldt Current did not exist during the middle Eocene (Marty et al., 1988). However, evidence from the deep-sea sediments of the Atlantic Ocean indicates that deep currents driven by cold and salty water masses from the Southern Ocean were already present during the Eocene (Oberhänsli et al., 1991). These southern-sourced cold bottom water was observed after 44 Ma (Zone P12) in the central southern Atlantic (Oberhänsli et al., 1991). After 36 Ma (Zone P15), when evidence for glaciations in Antarctica also becomes extensive (Hutchinson et al., 2021), this cold bottom water starts being recorded in most of the Atlantic (Oberhänsli et al., 1991). This is consistent with: (i) a benthic foraminiferal fauna and stable isotope ratios suggesting that a southern source of deep, cold waters may have functioned even earlier (Pak and Miller, 1992); and (ii) the beginning of deep circulation in the North Atlantic around 44 Ma (Vahlenkamp et al., 2018). Consistently, around 43 Ma, a weak, cool upwelling current may have bathed the coasts of the Pisco Basin, favoring a moderate nutrient enrichment as well as a relevant abundance of heterotroph carbonate producers. The resulting subtropical to warm-temperate carbonate factory testifies to the initial steps of the

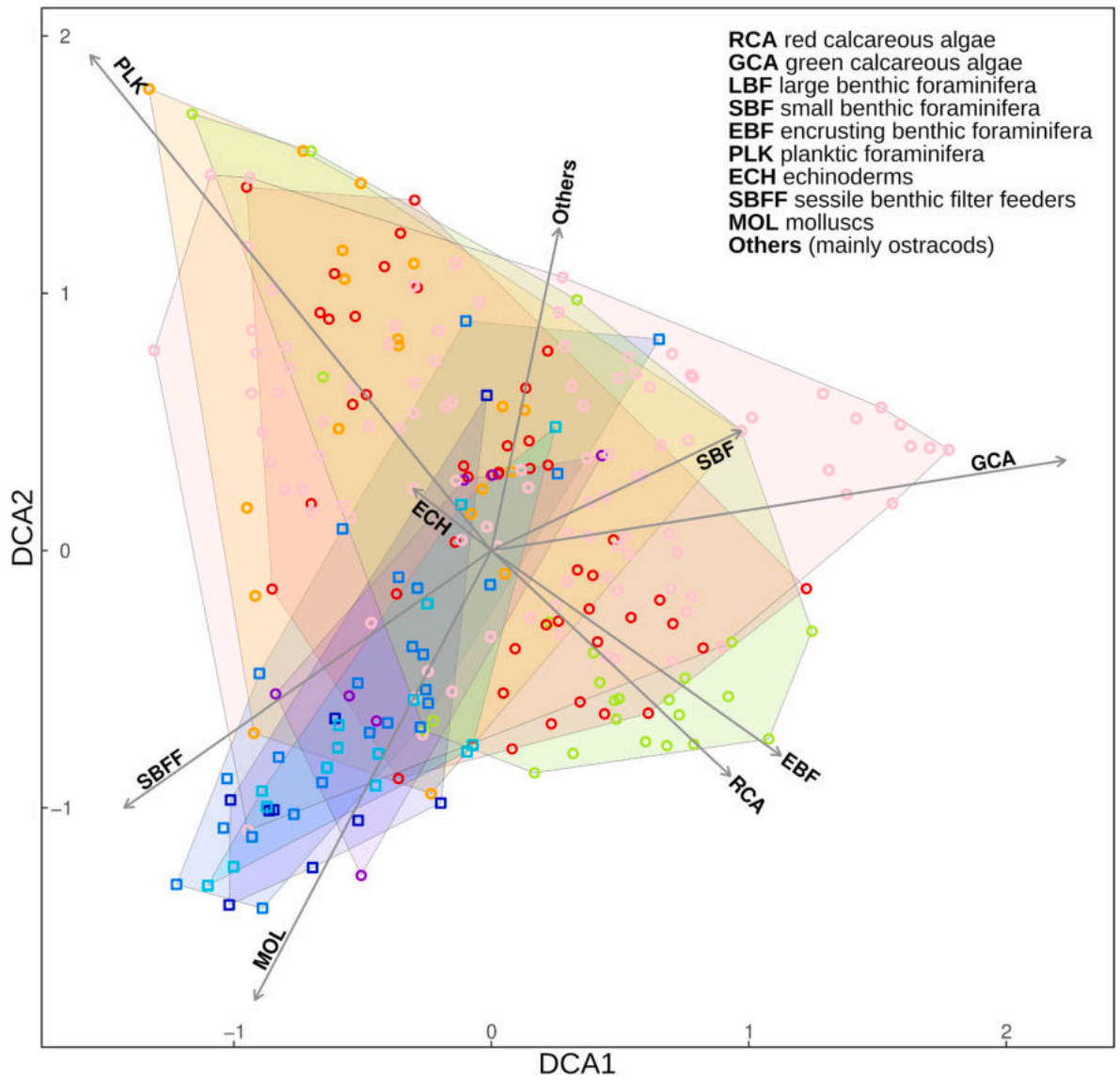

Fig. 12. DCA plot of the skeletal assemblages of the various samples from the Pisco Basin (squares) and from Tethys (circles), the plot displays the same acronyms as Fig. 11.

progressive cooling and nutrient enrichment of the Peruvian coastal water. Therefore, notwithstanding its tropical latitudinal setting, the Paracas Formation did not form under fully tropical paleoclimatic conditions. This is also supported by the overall warm-temperate affinities of the microfossil assemblages from the Yumaque Member, which represents the offshore counterpart of the underlying Los Choros strata (Malinverno et al., 2021). The cooling trend would persists through most of the Cenozoic as highlighted by the Priabonian diatomaceous layers of the upper Otuma Formation (Malinverno et al., 2021), the Aquitanian diatomites of the Tunga Formation (DeVries et al., 2024), the Burdigalian heterozoan-dominated factories of the lower Chilcatay Formation (Coletti et al., 2018b), and the Middle and Late Miocene diatomites of the Pisco Formation (Malinverno et al., 2025).

The LBF-rich deposits of the Los Choros Member thus represent a slightly cooler and slightly nutrient-richer version of the Eocene LBF-rich deposits from Tethys, as displayed by their large overlap in the ordination space (Figs. 11 and 12). In particular, the lepidocyclinids-and-mollusks biofacies display a striking similarity, in terms of skeletal assemblage, texture and mineralogical composition, with the nummulitid biofacies (sensu Coletti et al., 2021a; Mariani et al., 2024) (Table 3).

The two biofacies also exhibit comparable abundances of orthophragminids, one of the few LBF groups present in both Pisco Basin and European sites. This overall closeness suggests an ecological similarity between the two dominating types of LBF of these biofacies: *Nummulites* and lepidocyclinids. Indeed, both *Nummulites* and most lepidocyclinids (with the possible exception of the largest *Eulepidina* species) preferentially inhabited outer-inner to outer-middle shelf tropical settings (Sinclair et al., 1998; Nebelsick et al., 2005; Mitchell et al., 2022) and displayed the ability to endure significant inputs of clastics (e.g., Lokier et al., 2009; Briguglio et al., 2021). Such a congruent autecology likely triggered competition wherever and whenever these two groups co-occurred within the same area. Examples of this may be seen in both bioprovinces. In America, where the two group coexisted for more than 30 million years (Mitchell et al., 2024), *Nummulites* does not occur with the plethora of species that used to inhabit the Eurasian province, nor it ever became a massive carbonate producer as it did in the Tethys (Schaub, 1983; BouDagher-Fadel and Price, 2014; Mitchell et al., 2024). In Eurasia, the lepidocyclinids became widespread during the late Rupelian (Cahuzac and Poignant, 1997; Dill et al., 2020). Before the end of the Chattian, that is no more than three million years after the earliest evidence for the arrival of lepidocyclinids, the 28 million-year-long

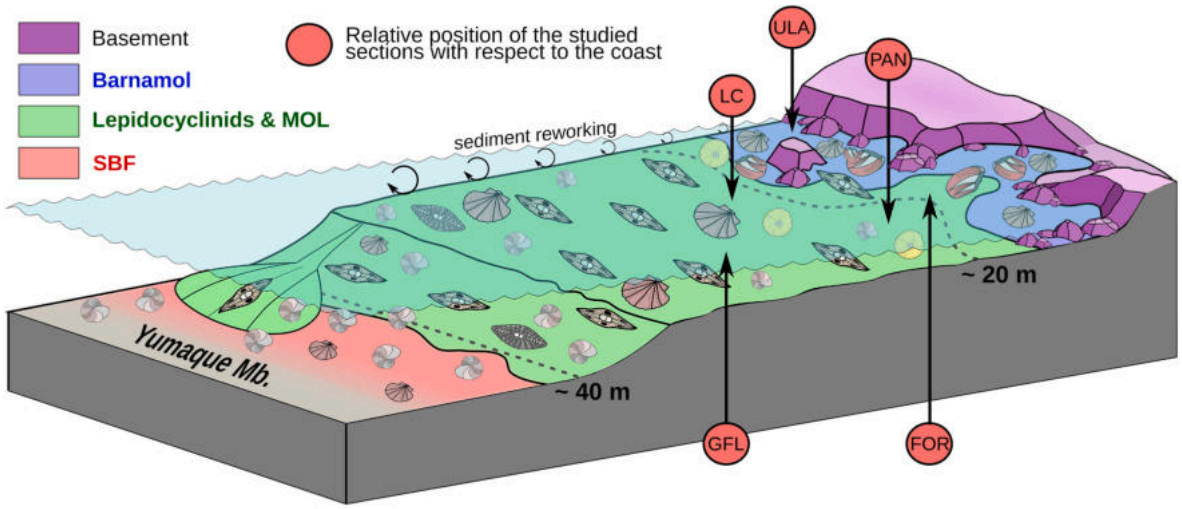

Fig. 13. Schematic paleoenvironmental reconstruction of the middle Eocene Los Choros Member of the Paracas Formation at the beginning of the marine transgression, later stages of the cycle are characterized by a more uniform deposition of the Yumaque Member. The key to the symbols is the same as in Fig. 3.

Table 3
Skeletal and mineralogical composition of the lepidocyclinids and mollusks biofacies (this work) and the nummulitid biofacies (Coletti et al., 2021a; Mariani et al., 2024).

	Lepidocyclinids and mollusks biofacies (this work)	Nummulitid biofacies (Coletti et al., 2021a; Mariani et al., 2024)
Mineralogical composition (QXRD)		
Silicates	40.0	17.0
Carbonates	60.0	83.0
Skeletal assemblage (% point counting)		
Calcareous algae	0.5	2.0
LBF	60	60
Encrusting benthic foraminifera	0.5	0.5
SBF	9.5	10.5
Planktic foraminifera	0.0	1.0
Mollusks	18.0	5.5
Barnacles	7.0	0.0
Echinoderms	3.5	7.0
Bryozoans	0.5	1.0
Other heterotrophs	0.5	8.5
Benthic heterotrophs vs benthic phototrophs	**1.70**	**1.90**
Orthophragminids vs lepidocyclinids/ nummulitids	**0.05**	**0.03**

history of the rock-forming *Nummulites* species was over (Cahuzac and Poignant, 1997). The timing of the final demise of *Nummulites* in the Tethys and the scarcity of *Nummulites*-dominated biogenic carbonates in the American province suggests that lepidocyclinids were able to outcompete *Nummulites* in most shallow-marine habitats. Because both taxa were primarily found at middle shelf depths, their light requirements were probably similar, and the reason for the eventual success of the lepidocyclinids must be connected to something else. Here, a significant clue is once again provided by the skeletal assemblages of the Pisco Basin, where lepidocyclinids thrived despite the mesotrophic cool-subtropical conditions. This is consistent with the purported evolutionary origin of the lepidocyclinids, which are believed to descend from an amphistigenid ancestor (BouDagher-Fadel and Price, 2010; BouDagher-Fadel, 2018). *Amphistegina* is the most thermally tolerant genus among the extant hyaline LBF (Langer and Hottinger, 2000). Conversely, most of recent nummulitids are strictly tropical (Beavington-Penney and Racey, 2004). *Nummulites* began becoming widespread in the Tethys as a consequence of the Paleocene–Eocene Thermal Maximum (Ali et al., 2025; Pujalte et al., 2025). *Nummulites* diversity peaked during the middle Eocene (Benedetti and Papazzoni, 2022), and began to decline during the colder late Eocene, first and foremost with the disappearance of the giant-sizes species (BouDagher-Fadel and Price, 2014), highlighting an overall preference for very warm temperatures.

Assuming that lepidocyclinids were generally able to outcompete *Nummulites* across most shelf settings, likely due to their greater eurythermy, it remains to be explained why they did not colonize the Eurasian province until Oligocene times. During the Eocene, the Atlantic Ocean became progressively wider, and the existing shoals and islands occurring between the South American and African coasts (e.g., those belonging to the Rio Grande Rise) sank progressively (Oliveira et al., 2009). Therefore, crossing the Atlantic would have been easier during the Eocene than in the Oligocene, and particularly in middle Eocene times. This is clearly testified by the distribution patters of semiaquatic and terrestrial mammals such as the archaic four-legged cetaceans in the family Protocetidae and the caviomorph rodents, which reached South America from Africa not later than the early middle Eocene and slightly before the beginning of the Oligocene, respectively (e.g., Flynn et al., 2003; Lambert et al., 2019), as well as by the dispersal of other LBF from America to Africa during the Eocene (Özcan et al., 2019). That said, why did lepidocyclinids only begin to spread in Eurasia around the end of the Rupelian, and not earlier? Once again, the answer to this enigma may be related to global temperatures, which remained high during the middle Eocene, marginally decreased in late Eocene times, and significantly decreased only during the early Oligocene (Westerhold et al., 2020). As suggested by BouDagher-Fadel and Price (2014), lepidocyclinids may have crossed the Atlantic to reach Africa as early as in Eocene times. However, shaking the well-established *Nummulites*-dominated carbonate assemblages of the Tethys would have been quite difficult at a time of high global temperatures, which accounts for the temporary failure of these "American immigrants" in the Tethys Ocean. When temperatures dropped during the Oligocene, the thermal tolerance of lepidocyclinids became the key to their success and widespread proliferation, which first displaced and then fostered the eventual fall of the *Nummulites*-dominated carbonate assemblages.

6. Conclusions

The Paleogene record of the Pisco Basin provides a vital window into the shelf carbonate factories of the tropical proto-Pacific, complementing the knowledge issued from its marine vertebrate assemblage. The coarse-grained, mixed siliciclastic-bioclastic deposits of the Los Choros Member formed in the middle Eocene (ca. 43 Ma) during a marine

transgression over the crystalline basement of the developing East Pisco forearc basin. Although deposited at tropical latitudes, this shallow-water unit is rich in heterotrophic benthic carbonate producers, including significant accumulations of acorn barnacles. This suggests subtropical to warm-temperate conditions and mesotrophic coastal waters, likely resulting from a weak coastal upwelling regime that was primarily driven by the effect of trade winds (though a minor contribution from deep water circulation cannot be completely ruled out).

Three main biofacies were recognized. A mollusk-dominated, barnacle- and siliciclastic-rich biofacies, comprised the nearshore belt of sedimentary deposits, bordering the rugged coastline and extending between 0 and 20 m water depth. This high-energy setting would have allowed for significant abrasion rates and in situ reworking of the bioclasts. Slightly further away from the coast, carbonate production was dominated by lepidocyclinids and mollusks. Large benthic foraminifera represented the overwhelmingly dominant protozoan component of this facies, which developed at water depths most likely comprised between 15 and 40 m, where the seafloor was still affected by waves, allowing for minor in situ reworking of the clasts and occasional offshore transport of smaller grains. Further offshore carbonate production was dominated by small benthic foraminifera, including abundant bolivinitids and nonionids, both of which are infaunal taxa that can tolerate organic matter enrichment and thrive over a wide depth range. Common mixed assemblages testify to an overall ramp-like submerged topography featuring no relevant barriers to the downdip movement of skeletal fragments.

Overall, the observed shallow-marine biofacies exhibit striking similarities to coeval shallow-water biofacies of the Tethys. Such similarities are especially obvious between the Peruvian lepidocyclinids-and-mollusks biofacies and the Tethyan nummulitid biofacies. This evokes comparable ecological preferences between the two dominant groups of benthic foraminifera, namely, lepidocyclinids and *Nummulites*, which in turn may have caused competition between the two groups wherever they lived sympatrically. Their overall distribution patterns suggest that lepidocyclinids were able to outcompete *Nummulites* thanks to their broader thermal tolerance, which was probably inherited from their amphisteginid ancestors. During the Oligocene cooling, lepidocyclinids successfully colonized the Tethys, which was previously dominated by the more stenothermal *Nummulites*, ultimately rendering the latter geologically insignificant in terms of carbonate production. Preliminary as it is, this evidence frames the Tethys Oligocene LBF turnover as a prominent example of an "invasive" carbonate producer causing significant and irreversible changes in carbonate factories.

Declaration of generative AI and AI-assisted technologies in the writing process

During the preparation of this work the authors used Gemini (Google) in order to support the refinement of narrative structure, clarity of expression, and adherence to journal formatting guidelines. After using this tool, the authors reviewed and edited the content as needed and take full responsibility for the content of the publication.

CRediT authorship contribution statement

Giovanni Coletti: Conceptualization, Data curation, Formal analysis, Investigation, Methodology, Resources, Supervision, Validation, Visualization, Writing – original draft, Writing – review & editing. **Luca Mariani:** Conceptualization, Data curation, Formal analysis, Investigation, Methodology, Resources, Supervision, Validation, Visualization, Writing – original draft, Writing – review & editing. **Elisa Malinverno:** Conceptualization, Formal analysis, Investigation, Methodology, Resources, Supervision, Validation, Writing – review & editing. **Alberto Vimercati:** Formal analysis, Investigation, Software, Writing – review & editing. **Claudio Di Celma:** Formal analysis, Investigation, Supervision, Writing – review & editing. **Alberto Collareta:** Conceptualization, Funding acquisition, Investigation, Project administration, Resources, Supervision, Writing – review & editing. **Giancarlo Molli:** Formal analysis, Investigation, Resources, Supervision, Writing – review & editing. **Giovanni Sarti:** Investigation, Writing – review & editing. **Giovanni Bianucci:** Formal analysis, Investigation, Supervision, Writing – review & editing. **Orangel Aguilera:** Supervision, Validation, Writing – review & editing. **Alessandro Cavallo:** Formal analysis, Methodology, Validation, Writing – review & editing. **Mario Urbina:** Formal analysis, Investigation, Resources, Writing – review & editing. **Giulia Bosio:** Conceptualization, Data curation, Formal analysis, Investigation, Methodology, Resources, Supervision, Validation, Visualization, Writing – original draft, Writing – review & editing.

Declaration of competing interest

The authors declare that they have no known competing financial interests or personal relationships that could have appeared to influence the work reported in this paper.

Acknowledgments

We acknowledge financial support by the European Union – NextGenerationEU, Mission 4, Component 2 CUP I53D23002070 006. Project Title: BIOVERTICES (BIOdiversity of VERTebrates In the CEnozoic Sea). This project is also supported by the University of Pisa under the ProArcheo 2024 Call for co-funding of Archaeological and Geopaleontological re-search. L.M. is grateful to the PhD program of the Department of Earth and Environmental Sciences of Milano Bicocca University for supporting this research. The authors thank two anonymous reviewers and the editor (F. Vega) for their constructive remarks. The authors are also grateful to Andrea Benedetti, Simon Mitchell and Edward Robinson for their remarkable scientific contributions to larger benthic foraminiferal paleontology which represents the foundation of the current research, and to W. Aguirre, J. Chauca-Luyo, and R. M. Varas for their assistance in the field. Finally, the first author wishes to dedicate a special acknowledgment to the late Silvia Spezzaferri, whose remarkable ability to connect and guide young researchers lies at the heart of this work.

Appendix A. Supplementary data

Supplementary data to this article can be found online at https://doi.org/10.1016/j.jsames.2026.105983.

Data availability

All the relevant data are included in the main text of the paper itself and its supplementary.

References

Adams, C.G., 1987. On the classification of the Lepidocyclinidae (Foraminifera) with redescription of the unrelated Paleocene genera *Actinosiphon* and *Orbitosiphon*. Micropaleontology 33, 289–317.

Agnini, C., Fornaciari, E., Raffi, I., Catanzariti, R., Pälike, H., Backman, J., Rio, D., 2014. Biozonation and biochronology of Paleogene calcareous nannofossils from low and middle latitudes. Newslett. Stratigr. 47 (2), 131–181.

Aguilera, O., Bencomo, K., de Araújo, O.M.O., Dias, B.B., Coletti, G., Lima, D., Silane, A. F., Polk, M., Alves-Martin, M.V., Jaramillo, C., Kutter, V.T., Lopes, R.T., 2020. Miocene heterozoan carbonate systems from the western Atlantic equatorial margin in South America: the Pirabas formation. Sediment. Geol. 407, 1–28. https://doi.org/10.1016/j.Sedgeo.2020.105739.

Ali, M., Coletti, G., Garzanti, E., Adatte, T., Castelltort, S., Sternai, P., Benedetti, A., Malinverno, E., Mariani, L., Spangerberg, J.E., Khan, S., Basso, D., Samankassou, E., Kocsis, L., Usman, M., 2025. The Baroch Nala section (NE Pakistan): a new PETM standard for the eastern Tethys. Mar. Petrol. Geol. 171, 107183.

Beavington-Penney, S.J., Racey, A., 2004. Ecology of extant nummulitids and other larger benthic foraminifera: applications in palaeoenvironmental analysis. Earth Sci. Rev. 67 (3–4), 219–265.

Benedetti, A., 2015. The New Family Ornatorotaliidae (Rotaliacea, Foraminiferida). Micropaleontology, pp. 231–236.

Benedetti, A., Marino, M., Pichezzi, R.M., 2018. Paleocene to lower Eocene larger foraminiferal assemblages from Central Italy: new remarks on biostratigraphy. Riv. Ital. Paleontol. Stratigr. 124 (1).
Benedetti, A., Papazzoni, C.A., Bosellini, F.R., 2024. Unparallel resilience of shallow-water tropical calcifiers (foraminifera and scleractinian reef corals) during the early Paleogene global warming intervals. Palaeogeogr. Palaeoclimatol. Palaeoecol. 651, 112393.
Benedetti, A., Papazzoni, C.A., 2022. Rise and fall of rotaliid Foraminifera across the Paleocene and Eocene times. Micropaleontology 68 (2), 185–196.
Bialik, O.M., Coletti, G., Mariani, L., Commissario, L., Desbiolles, F., Meroni, A.N., 2023. Availability and type of energy regulate the global distribution of neritic carbonates. Sci. Rep. 13 (1), 19687.
Bialik, O.M., Jarochowska, E., Grossowicz, M., 2021. Ordination analysis in sedimentology, geochemistry and palaeoenvironment—Background, current trends and recommendations. Deposit. Record 7 (3), 541–563.
Bianucci, G., Collareta, A., Bosio, G., Landini, W., Gariboldi, K., Gioncada, A., Lambert, O., Malinverno, E., de Muizon, C., Varas-Malca, R., Villa, I.M., Coletti, G., Urbina, M., Di Celma, C., 2018. Taphonomy and palaeoecology of the lower Miocene marine vertebrate assemblage of Ullujaya (Chilcatay Formation, East Pisco Basin, southern Peru). Palaeogeogr. Palaeoclimatol. Palaeoecol. 511, 256–279.
Bianucci, G., Lambert, O., Urbina, M., Merella, M., Collareta, A., Bennion, R., Salas-Gismondi, R., Benites-Palomino, A., Post, K., de Muizon, C., Bosio, G., Di Celma, C., Malinverno, E., Pierantoni, P.P., Villa, I.M., Amson, E., 2023. A heavyweight early whale pushes the boundaries of vertebrate morphology. Nature 620 (7975), 824–829.
Bianucci, G., Collareta, A., 2022. An overview of the fossil record of cetaceans from the East Pisco Basin (Peru). Boll. Soc. Paleontol. Ital. 61 (1), 19–20.
Bosellini, A., Russo, A., Arush, M.A., Cabdulqadir, M.M., 1987. The Oligo-Miocene of Eil (NE Somalia): a prograding coral-lepidocyclina system. J. Afr. Earth Sci. 6 (4), 583–593.
Bosellini, F.R., Benedetti, A., Kiessling, W., 2025. Minor coral diversity loss but long-lasting coral reef crises in the early Paleogene hothouse. Paleoceanogr. Paleoclimatol. 40 (3).
Bosio, G., Collareta, A., Di Celma, C., Lambert, O., Marx, F.G., Muizon, C. de, Gioncada, A., Gariboldi, K., Malinverno, E., Varas-Malca, R., Urbina, M., Bianucci, G., 2021. Taphonomy of marine vertebrates of the Pisco Formation (Miocene, Peru): insights into the origin of an outstanding Fossil-Lagerstätte. PLoS One 16, e0254395.
Bosio, G., Collareta, A., Pedini, M., Gastaldello, M.E., Nobile, F., Pellegrino, L., Pierantoni, P., Malinverno, E., Lambert, O., Marrama, G., Landini, W., Carnevale, G., Varas-Malca, R., Di Celma, C., Mazzoli, S., Urbina, M., Bianucci, G., 2025a. Miocene stratigraphy and vertebrate paleontology along the western side of Cerros Cadena de los Zanjones (East Pisco Basin, Peru). J. Maps 21 (1), 2472779.
Bosio, G., Collareta, A., Pellegrino, L., Bianucci, G., Insacco, G., Coletti, G., 2025b. Barnacle taphonomy and ultrastructure: comparing modern and fossil shells from the western Mediterranean. Lethaia 58 (3), 1–21.
BouDagher-Fadel, M.K., 2018. Evolution and Geological Significance of Larger Benthic Foraminifera. University College London Press, London.
BouDagher-Fadel, M.K., Price, G.D., 2010. Evolution and paleogeographic distribution of the lepidocyclinids. J. Foraminifer. Res. 40, 79–108.
BouDagher-Fadel, M.K., Price, G.D., 2014. The phylogenetic and palaeogeographic evolution of the nummulitoid larger benthic Foraminifera. Micropaleontology 483–508.
Bown, P.R., Young, J.R., 1998. Techniques. In: Bown, P.R. (Ed.), Calcareous Nannofossil Biostratigraphy. Chapman and Hall, London, pp. 16–28.
Bray, J.R., Curtis, J.T., 1957. An ordination of the upland Forest communities of Southern Wisconsin. Ecol. Monogr. 27, 325–349. https://doi.org/10.2307/1942268.
Briguglio, A., Vannucci, G., Bruzzone, C., Piazza, M., 2021. Stratigraphic development of a late oligocene reef complex under strong fluviatile influence in the tertiary piedmont basin (Liguria, NW Italy). Micropaleontology 67 (4), 315–339.
Buckeridge, J.S., Lee, D.E., Robinson, J.H., 2014. A diverse shallow-water barnacle assemblage (Cirripedia: Sessilia) from the Oligocene of Southland, New Zealand. N. Z. J. Geol. Geophys. 57 (2), 253–263.
Butterlin, J., 1984. Notes on some larger Foraminifera from the Tertiary of the French Lesser Antilles and on the phylogeny of American species of the genus Lepidocyclina. Bull. Cent. Rech. Explor.-Prod. Elf-Aquitaine 6, 105–115.
Butterlin, J., 1990. Problèmes poses par la systematique de la famille Lepidocyclinidae (Foraminiferida). Rev. Espanola Micropaleontol. 22, 101–126.
Cahuzac, B., Poignant, A., 1997. Essai de biozonation de l'Oligo-Miocène dans les bassins européens à l'aide des grands foraminifères néritiques. Bull. Soc. Geol. Fr. 168 (2), 155–169.
Ciattoni, S., Cella, F., Mazzoli, S., Zambrano, M., Megna, A., Santini, S., Butler, R., Pierantoni, P.P., Di Celma, C., 2025. Lithosphere architecture along the axis of the subducting aseismic Nazca Ridge (Peruvian active margin). Tectonics 44 (1).
Coletti, G., Balmer, E.M., Bialik, O.M., Cannings, T., Kroon, D., Robertson, A.H., Basso, D., 2021b. Microfacies evidence for the evolution of Miocene coral-reef environments in Cyprus. Palaeogeogr. Palaeoclimatol. Palaeoecol. 584, 110670.
Coletti, G., Bosio, G., Collareta, A., Bialik, O.M., Regattieri, E., Cornacchia, I., Insacco, G., Buckeridge, J., 2024. Barnacle-rich facies as a tool for palaeoenvironmental reconstructions. Palaeogeogr. Palaeoclimatol. Palaeoecol. 634, 111914.
Coletti, G., Bosio, G., Collareta, A., Buckeridge, J., Consani, S., El Kateb, A., 2018b. Palaeoenvironmental analysis of the Miocene barnacle facies: case studies from Europe and South America. Geol. Carpathica 69 (6), 573–592.
Coletti, G., Bosio, G., Collareta, A., Malinverno, E., Bracchi, V.A., Di Celma, C., Basso, D., Stainbank, S., Spezzaferri, S., Cannings, T., Bianucci, G., 2019. Biostratigraphic, evolutionary, and paleoenvironmental significance of the southernmost lepidocyclinids of the Pacific coast of South America (East Pisco Basin, southern Peru). J. S. Am. Earth Sci. 96, 102372.
Coletti, G., Commissario, L., Ali, M., Mariani, L., Granier, B., Brandano, M., Mancini, A., Rusciadelli, G., Ricci, C., Baceta, J.I., Mateu-Vicens, G., Basso, D., 2025. Coral carbonate production during the Paleocene: insights from the Maiella Massif (Pennapiedimonte, Central Italy). Riv. Ital. Paleontol. Stratigr. 131 (1), 177–200.
Coletti, G., Commissario, L., Mariani, L., Bosio, G., Desbiolles, F., Soldi, M., Bialik, O.M., 2022. Palaeocene to Miocene southern Tethyan carbonate factories: a meta-analysis of the successions of South-western and Western Central Asia. Deposit. Record 8 (3), 1031–1054.
Coletti, G., Mariani, L., Garzanti, E., Consani, S., Bosio, G., Vezzoli, G., Hu, X., Basso, D., 2021a. Skeletal assemblages and terrigenous input in the Eocene carbonate systems of the Nummulitic Limestone (NW Europe). Sediment. Geol. 425, 106005.
Coletti, G., Stainbank, S., Fabbrini, A., Spezzaferri, S., Foubert, A., Kroon, D., Betzler, C., 2018a. Biostratigraphy of large benthic Foraminifera from Hole U1468A (Maldives): a CT-scan taxonomic approach. Swiss J. Geosci. 111 (3), 523–536.
Collareta, A., Lambert, O., Landini, W., Di Celma, C., Malinverno, E., Varas-Malca, R., Urbina, M., Bianucci, G., 2017. Did the giant extinct shark *Carcharocles megalodon* target small prey? Bite marks on marine mammal remains from the late Miocene of Peru. Palaeogeogr. Palaeoclimatol. Palaeoecol. 469, 84–91.
DeVries, T.J., 1998. Oligocene deposition and Cenozoic sequence boundaries in the Pisco Basin (Peru). J. S. Am. Earth Sci. 11 (3), 217–231.
DeVries, T.J., 2017. Eocene stratigraphy and depositional history near Puerto Caballas (East Pisco Basin, Peru). Bol. Soc. Geol. Peru 112, 39–52.
DeVries, T.J., 2019. Early Paleogene brackish-water molluscs from the Caballas Formation of the East Pisco Basin (southern Peru). J. Nat. Hist. 53 (25–26), 1533–1584.
DeVries, T.J., Barron, J.A., Ochoa, D., McDougall, K., 2024a. Chronology and Paleoenvironment of the Tunga Formation, a new lowermost Miocene sequence in the East Pisco Basin of southern Peru. Stratigraphy 21 (3), 189–224.
DeVries, T.J., Barron, J.A., Ochoa, D., McDougall, K., 2024b. Chronology and paleoenvironment of the Tunga Formation, a new lowermost Miocene sequence in the East Pisco Basin of southern Peru. Stratigraphy (3), 190–225.
DeVries, T.J., Narváez, Y., Sanfilippo, A., Malumian, N., Tapia, P., 2006. New microfossil evidence for a late Eocene age of the Otuma Formation (Southern Peru). In: XIII Congreso Peruano De Geología, pp. 615–618.
DeVries, T.J., Urbina, M., Jud, N.A., 2017. The Eocene-Oligocene Otuma depositional sequence (East Pisco Basin, Peru): paleogeographic and paleoceanographic implications of new data. Bol. Soc. Geol. Peru 112, 14–38.
DeVries, T.J., Jud, N.A., 2018. Lithofacies patterns and paleogeography of the Miocene Chilcatay and lower Pisco depositional sequences (East Pisco Basin, Peru). Bol. Soc. Geol. Peru 8, 124–167.
Di Celma, C., Pierantoni, P.P., Volatili, T., Molli, G., Mazzoli, S., Sarti, G., Ciattoni, S., Bosio, G., Malinverno, E., Collareta, A., Gariboldi, K., Gioncada, A., Jablonska, D., Landini, W., Urbina, M., Bianucci, G., 2022. Towards deciphering the Cenozoic evolution of the East Pisco Basin (southern Peru). J. Maps 18 (2), 397–412.
Dill, M.A., Vaziri-Moghaddam, H., Seyrafian, A., Behdad, A., Shabafrooz, R., 2020. A review of the Oligo–Miocene larger benthic Foraminifera in the Zagros basin, Iran; new insights into biozonation and palaeogeographical maps. Rev. Micropaleontol. 66, 100408.
Donovan, S.K., 1993. The ecology of ancient barnacles. Rocks Miner. 68 (2), 115–119.
Dunbar, R.B., Marty, R.C., Baker, P.A., 1990. Cenozoic marine sedimentation in the Sechura and Pisco basins, Peru. Palaeogeogr. Palaeoclimatol. Palaeoecol. 77 (3–4), 235–261.
Eames, F.E., Banner, F.T., Blow, W.H., Clarke, W.J., Smout, A.H., 1962. Morphology, taxonomy, and stratigraphic occurrence of the Lepidocyclininae. Micropaleontology 8 (3), 289–322.
Faul, K.L., Ravelo, A.C., Delaney, M.L., 2000. Reconstructions of upwelling, productivity, and photic zone depth in the eastern equatorial Pacific Ocean using planktonic foraminiferal stable isotopes and abundances. J. Foraminifer. Res. 30 (2), 110–125.
Flügel, E., Munnecke, A., 2010. Microfacies of Carbonate Rocks: Analysis, Interpretation and Application, vol 976. springer, Berlin, p. 2004.
Flynn, J.J., Wyss, A.R., Croft, D.A., Charrier, R., 2003. The Tinguiririca fauna, Chile: biochronology, paleoecology, biogeography, and a new earliest Oligocene South American land mammal 'age'. Palaeogeogr. Palaeoclimatol. Palaeoecol. 195 (3–4), 229–259.
Fornaciari, E., Agnini, C., Catanzariti, R., Rio, D., Bolla, M.E., Valvasoni, E., 2010. Mid-latitude calcareous nannofossil biostratigraphy and biochronology across the middle to late Eocene transition. Stratigraphy 7, 229–264.
Gauch, Jr H.G., Whittaker, R.H., 1972. Coenocline simulation. Ecology 53 (3), 446–451.
Geel, T., 2000. Recognition of stratigraphic sequences in carbonate platform and slope deposits: empirical models based on microfacies analysis of Palaeogene deposits in southeastern Spain. Palaeogeogr. Palaeoclimatol. Palaeoecol. 155 (3–4), 211–238.
Gualtieri, A.F., 2000. Accuracy of XRPD QPA using the combined Rietveld–RIR method. J. Appl. Crystallogr. 33, 267–278.
Hallock, P., Schlager, W., 1986. Nutrient excess and the demise of coral reefs and carbonate platforms. Palaios 389–398.
Hampel, A., 2002. The migration history of the Nazca Ridge along the Peruvian active margin: a re-evaluation. Earth Planet Sci. Lett. 203 (2), 665–679.
Hayward, B.W., 2002. Late Pliocene to middle Pleistocene extinctions of deep-sea benthic Foraminifera ("*Stilostomella* extinction") in the southwest Pacific. J. Foraminifer. Res. 32 (3), 274–307.
Hill, M.O., Gauch Jr, H.G., 1980. Detrended correspondence analysis: an improved ordination technique. Vegetatio 42 (1), 47–58.
Hottinger, L., Bassi, D., 2014. Paleogene Larger Rotaliid Foraminifera from the Western and Central Neotethys. Springer, Berlin, pp. 3–191.

Hsu, J.T., 1992. Quaternary uplift of the Peruvian coast related to the subduction of the Nazca Ridge: 13.5 to 15.6 degrees south latitude. Quat. Int. 15, 87–97.
Hutchinson, D.K., Coxall, H.K., Lunt, D.J., Steinthorsdottir, M., de Boer, A.M., Baatsen, M., von der Heydt, A., Huber, M., Kennedy-Asser, A.T., Kunzmann, L., Ladant, J.-B., Lear, C.H., Moraweck, K., Pearson, P.N., Piga, E., Pound, M.J., Salzmann, U., Scher, H.D., Sijp, W.P., Śliwińska, K.K., Wilson, P.A., Zhang, Z., 2021. The Eocene–Oligocene transition: a review of marine and terrestrial proxy data, models and model–data comparisons. Clim. Past 17, 269–315.
Kruskal, J.B., 1964. Nonmetric multidimensional scaling: a numerical method. Psychometrika 29 (2), 115–129.
Kulm, L.D., Thornburg, T.M., Schrader, H.J., Resig, J.M., 1982. Cenozoic structure, stratigraphy and tectonics of the central Peru forearc. Geol. Soc. London, Spec. Publ. 10 (1), 151–169.
Lambert, O., Bianucci, G., Post, K., De Muizon, C., Salas-Gismondi, R., Urbina, M., Reumer, J., 2010. The giant bite of a new raptorial sperm whale from the Miocene epoch of Peru. Nature 466 (7302), 105–108.
Lambert, O., Bianucci, G., Salas-Gismondi, R., Di Celma, C., Steurbaut, E., Urbina, M., de Muizon, C., 2019. An amphibious whale from the Middle Eocene of Peru reveals early South Pacific dispersal of quadrupedal cetaceans. Curr. Biol. 29, 1352–1359.
Lambert, O., Martínez-Cáceres, M., Bianucci, G., Di Celma, C., Salas-Gismondi, R., Steurbaut, E., Urbina, M., de Muizon, C., 2017. Earliest mysticete from the Late Eocene of Peru sheds new light on the origin of baleen whales. Curr. Biol. 27, 1535–1541 e2.
Langer, M.R., Hottinger, L., 2000. Biogeography of selected" larger" Foraminifera. Micropaleontology 46, 105–126.
Larson, A.C., Von Dreele, R.B., 1994. Generalized Structure Analysis System, pp. 86–748. Report lAUR.
Legendre, P., Borcard, D., 2018. Box–Cox-chord transformations for community composition data prior to beta diversity analysis. Ecography 41 (11), 1820–1824.
Legendre, P., Gallagher, E.D., 2001. Ecologically meaningful transformations for ordination of species data. Oecologia 129, 271–280.
León, W., Aleman, A., Torres, V., Rosell, W., De La Cruz, O., 2008a. Estratigrafía, sedimentología y evolución tectónica de la cuenca Pisco oriental. Boletín INGEMMET 27, 144.
León, W., Aleman, A., Torres, V., Rosell, W., De La Cruz, O., 2008b. Estratigrafía, sedimentología y evolución tectónica de la cuenca Pisco Oriental. Boletín INGEMMET 27, 144.
Less, G., 1998. The zonation of the Mediterranean upper Paleocene and Eocene by Orthophragminae. Opera Dela Slovenska Akademija Znanosti in Umetnosti (4) 34 (2), 21–43.
Lisson, C.I., 1921. Contribución al estudio de algunos foraminferos terciarios provenientes de la región del norte del Peru. Asociación Peruviana Para El Progreso De Las Ciencias. Archivos 1, 1–53.
Lokier, S.W., Wilson, M.E., Burton, L.M., 2009. Marine biota response to clastic sediment influx: a quantitative approach. Palaeogeogr. Palaeoclimatol. Palaeoecol. 281 (1–2), 25–42.
Macharé, J., Ortlieb, L., 1992. Plio-Quaternary vertical motions and the subduction of the Nazca Ridge, central coast of Peru. Tectonophysics 205 (1–3), 97–108.
Malinverno, E., Bosio, G., Di Celma, C., Gariboldi, K., Gioncada, A., Pierantoni, P.P., Collareta, A., Molli, G., Bagnoli, G., Sarti, G., Urbina, M., Bianucci, G., 2021. (Bio) stratigraphic overview and paleoclimatic-paleoceanographic implications of the middle-upper Eocene deposits from the Ica River Valley (East Pisco Basin, Peru). Palaeogeogr. Palaeoclimatol. Palaeoecol. 578, 110567.
Malinverno, E., Bosio, G., Gastaldello, M., Pellegrino, L., Bianucci, G., Collareta, A., Gariboldi, K., Urbina, M., Villa, I.M., Di Celma, C., 2025. The early depositional history of the Pisco formation (middle to Upper Miocene, Peru). Newsl. Stratigr. 58 (1), 99–123.
Mariani, L., Coletti, G., Bosio, G., Vicens, G.M., Ali, M., Cavallo, A., Mittempergher, S., Malinverno, E., 2024. Tectonically-controlled biofacies distribution in the Eocene Foraminiferal Limestone (Pag, Croatia): a quantitative-based palaeontological analysis. Sediment. Geol. 472, 106743.
Marty, R., Dunbar, R., Martin, J.B., Baker, P., 1988. Late Eocene diatomite from the Peruvian coastal desert, coastal upwelling in the eastern Pacific, and Pacific circulation before the terminal Eocene event. Geology 16 (9), 818–822.
Mitchell, S., Robinson, E., Jiang, M.M., Robinson, N., Özcan, E., 2024. A larger benthic foraminiferal zonation for the Cenozoic of the Americas. Carnets Géol. 24, 163–172.
Mitchell, S.F., Robinson, E., Özcan, E., Jiang, M.M., Robinson, N., 2022. A larger benthic foraminiferal zonation for the Eocene of the Caribbean and central American region. Carnets Géol. 22 (11), 409–565.
Morales, M.C., Chacaltana, C., Valdiva, W., 2010. *Lepidocyclina* (*Lepidocyclina) Peruviana* (Cushman) En la Cuenca Pisco: Geocronologia Y Paleoambiente. Sociedad Geológica Del Perú, vol. 9. Spec. Publ., pp. 237–240
Morales, M.C., Tejada-Medina, L., Chacaltana, C., 2013. Significado de la presencia del foraminifero *Amphistegina* sp. Del Paleógeno en la Cuenca Pisco. I Simposio Internacional de Paleontologia del Perù 1, 29–32.
Mukasa, S.B., Henry, D.J., 1990. The San Nicolás batholith of coastal Peru: early Palaeozoic continental arc or continental rift magmatism? J. Geol. Soc. 147 (1), 27–39.
Murray, J.W., 2006. Ecology and Applications of Benthic Foraminifera. Cambrige University Press, Cambridge.
Muttoni, G., Gaetani, M., Kent, D.V., Sciunnach, D., Angiolini, L., Berra, F., Garzanti, E., Mattei, M., Zanchi, A., 2009. Opening of the Neo-Tethys Ocean and the Pangea B to Pangea A transformation during the Permian. GeoArabia (Manama) 14 (4), 17–48.
Nebelsick, J.H., Rasser, M.W., Bassi, D., 2005. Facies dynamics in Eocene to Oligocene circumalpine carbonates. Facies 51 (1), 197–217.
Oberhänsli, H., Müller-Merz, E., Oberhänsli, R., 1991. Eocene paleoceanographic evolution at 20–30 S in the Atlantic Ocean. Palaeogeogr. Palaeoclimatol. Palaeoecol. 83 (1–3), 173–215.
Oliveira, F.B.D., Molina, E.C., Marroig, G., 2009. Paleogeography of the South Atlantic: a route for primates and rodents into the New World?. In: South American Primates: Comparative Perspectives in the Study of Behavior, Ecology, and Conservation. Springer New York, New York, NY, pp. 55–68.
Ćosović, V., Drobne, K., 1995. Palaeoecological significance of morphology of orthophragminids from the Istrian Peninsula (Croatia and Slovenia). Geobios 28, 93–99.
Pak, D.K., Miller, K.G., 1992. Paleocene to Eocene benthic foraminiferal isotopes and assemblages: implications for deepwater circulation. Paleoceanography 7, 405–422.
Patacci, M., 2016. A high-precision Jacob's staff with improved spatial accuracy and laser sighting capability. Sediment. Geol. 335, 66–69.
Perch-Nielsen, K., 1985. Cenozoic calcareous nannofossils. In: Bolli, H.M., Saunders, J.B., Perch-Nielsen, K. (Eds.), Plankton Stratigraphy. Cambridge Earth Science Series, pp. 427–554.
Pomar, L., Baceta, J.I., Hallock, P., Mateu-Vicens, G., Basso, D., 2017. Reef building and carbonate production modes in the west-central Tethys during the Cenozoic. Mar. Petrol. Geol. 83, 261–304.
Pujalte, V., Payros, A., Orue-Etxebarria, X., Tosquella, J., Schmitz, B., Martínez-Braceras, N., 2025. Impact of the Paleocene-Eocene thermal maximum on the evolution of larger foraminifera: a new look at an old problem. Facies 71 (4), 19.
Ramos, V.A., 2008. The basement of the Central Andes: the Arequipa and related terranes. Annu. Rev. Earth Planet Sci. 36, 289–324.
Reymond, C.E., Zihrul, K.S., Halfar, J., Riegl, B., Humphreys, A., Westphal, H., 2016. Heterozoan carbonates from the equatorial rocky reefs of the Galápagos Archipelago. Sedimentology 63 (4), 940–958.
Rietveld, H.M., 1969. A profile refinement method for nuclear and magnetic structures. J. Appl. Crystallogr. 2, 65–71.
Romero, D., Valencia, K., Alarcón, P., Peña, D., Ramos, V.A., 2013. The offshore basement of Perú: evidence for different igneous and metamorphic domains in the forearc. J. S. Am. Earth Sci. 42, 47–60.
Schaub, H., 1983. Paleogene Tethys, domain of *Nummulites*. Boll. Soc. Paleontol. Ital. 22 (1–2), 93–102.
Sinclair, H.D., Sayer, Z.R., Tucker, M.E., 1998. Carbonate sedimentation during early foreland basin subsidence: the Eocene succession of the French Alps. Geological Society 149 (1), 205–227.
Sirel, E., Deveciler, A., 2017. A new late Ypresian species of *Asterigerina* and the first records of *Ornatorotalia* and *Granorotalia* from the Thanetian and upper Ypresian of Turkey. Riv. Ital. Paleontol. Stratigr. 123 (1).
Stampfli, G.M., 2000. Tethyan oceans. In: Bozkurt, E., Winchester, J.A., Piper, J.D.A. (Eds.), Tectonics and Magmatism in Turkey and the Surrounding Area, vol 173. Geological Society, London, Special Publications, pp. 1–23.1.
Syms, C., 2008. Principal Components Analysis. Elsevier.
Thornburg, T., Kulm, L.D., 1981. Sedimentary Basins of the Peru Continental Margin: Structure, Stratigraphy, and Cenozoic Tectonics from 6 S to 16 S Latitude.
Toby, B.H., 2001. EXPGUI, a graphical user interface for GSAS. J. Appl. Crystallogr. 34, 210–213.
Vaes, B., van Hinsbergen, D.J., van de Lagemaat, S.H., van der Wiel, E., Lom, N., Advokaat, E.L., Boschman, L.M., Gallo, L.C., Greve, A., Guilmette, C., Li, S., Lippert, P.C., Montheil, L., Qayyum, A., Langereis, C.G., 2023. A global apparent polar wander path for the last 320 Ma calculated from site-level paleomagnetic data. Earth Sci. Rev. 245, 104547.
Vahlenkamp, M., Niezgodzki, I., De Vleeschouwer, D., Bickert, T., Harper, D.T., Kirtland Turner, S., Lohmann, G., Sexton, P.F., Zachos, J.C., Pälike, H., 2018. Astronomically paced changes in deep-water circulation in the western North Atlantic during the middle Eocene. Earth Planet Sci. Lett. 484, 329–340.
Van de Geyn, W.A.E., Van der Vlerk, I.M., 1935. A monograph on the Orbitoididae, occurring in the Tertiary of America. Leidse Geol. Meded. 7 (1), 221–272.
Viveen, W., Schlunegger, F., 2018. Prolonged extension and subsidence of the Peruvian forearc during the Cenozoic. Tectonophysics 730, 48–62.
Wade, B.S., Pearson, P.N., Berggren, W.A., Pälike, H., 2011. Review and revision of Cenozoic tropical planktonic foraminiferal biostratigraphy and calibration to the geomagnetic polarity and astronomical time scale. Earth Sci. Rev. 104 (1–3), 111–142.
Westerhold, T., Marwan, N., Drury, A.J., Liebrand, D., Agnini, C., Anagnostou, E., Barnet, J.S.K., Bohaty, S.M., De Vleeschouwer, D., Florindo, F., Frederichs, T., Hodell, D.A., Holbourn, A.E., Kroon, D., Lauretano, V., Littler, K., Lourens, L.J., Lyle, M., Pälike, H., Röhl, U., Tian, J., Wilkens, R.H., Wilson, P.A., Zachos, J.C., 2020. An astronomically dated record of Earth's climate and its predictability over the last 66 million years. Science 369, 1383–1387. https://doi.org/10.1126/science.Aba6853.
Young, J.R., Bown, P.R., Lees, J.A., 2022. Nannotax3 website. International Nannoplankton Association. www.mikrotax.org/Nannotax3. (Accessed 10 June 2025).
Özcan, E., Mitchell, S.F., Less, G., Robinson, E., Bryan, J.R., Pignatti, J., Yücel, A.O., 2019. A revised suprageneric classification of American orthophragminids with emphasis on late Paleocene representatives from Jamaica and Alabama. J. Syst. Palaeontol. 17 (18), 1551–1579.
Özcan, E., Yücel, A.O., Erkızan, L.S., Gültekin, M.N., Kayğılı, S., Yurtsever, S., 2022. Atlas of the Tethyan orthophragmines. Mediterr. Geosci. Rev. 4 (1), 3–213.